university of groningen

University Medical Center Groningen

University of Groningen

Nanoparticles and stem cells for drug delivery to the brain

Stojanov, Katica

IMPORTANT NOTE: You are advised to consult the publisher's version (publisher's PDF) if you wish to cite from it. Please check the document version below.

Document Version
Publisher's PDF, also known as Version of record

Publication date:
2012

Link to publication in University of Groningen/UMCG research database

Citation for published version (APA):
Stojanov, K. (2012). *Nanoparticles and stem cells for drug delivery to the brain*. s.n.

Copyright
Other than for strictly personal use, it is not permitted to download or to forward/distribute the text or part of it without the consent of the author(s) and/or copyright holder(s), unless the work is under an open content license (like Creative Commons).

The publication may also be distributed here under the terms of Article 25fa of the Dutch Copyright Act, indicated by the "Taverne" license. More information can be found on the University of Groningen website: https://www.rug.nl/library/open-access/self-archiving-pure/taverne-amendment.

Take-down policy
If you believe that this document breaches copyright please contact us providing details, and we will remove access to the work immediately and investigate your claim.

Downloaded from the University of Groningen/UMCG research database (Pure): http://www.rug.nl/research/portal. For technical reasons the number of authors shown on this cover page is limited to 10 maximum.

Download date: 05-05-2023

Chapter 2

Imaging of cells and nanoparticles: implications for drug delivery to the brain

Katica Stojanov[1], Inge S. Zuhorn[1], Rudi A.J.O. Dierckx[2], Erik F. J. de Vries[2]

[1] Department of Cell Biology / Membrane Cell Biology, University Medical Center Groningen, University of Groningen, A. Deusinglaan 1, 9713 AV Groningen, the Netherlands
[2] Department of Nuclear Medicine and Molecular Imaging, University Medical Center Groningen, University of Groningen, Hanzeplein 1, 9713 GZ Groningen, The Netherlands

Under revision at Pharmaceutical Research

Abstract

A major challenge in the development of drugs for treatment of diseases of the central nervous system is to obtain drug concentrations inside the brain that reach therapeutic efficacy. Indeed, many efforts to accomplish such a goal have been frustrated because of poor brain penetration of potentially effective drugs, which has precluded their application in the clinic so far. However, to overcome this hurdle, devices are currently developed that may improve drug delivery into the brain. Among others, one approach involves the encapsulation of drugs into distinct nanocarriers that might be targeted (in)to the brain, followed by release of the drug. Alternatively, living cells have been engineered to produce the pharmaceutical of interest at the target site. To verify the efficiency of these drug delivery devices in reaching the brain, it is important to be able to follow their fate inside the body. Therefore, adequate methods to track these devices are required. To this end, both ex-vivo approaches and in-vivo imaging techniques are used, including ex-vivo biodistribution, autoradiography, magnetic resonance imaging, optical imaging, positron emission tomography and single photon computed emission tomography. Obviously, each method, however, has its specific advantages and limitations and consequently the selection of the tracking method should be based on the specific aims of the experiment. Here, we will discuss the ex-vivo and in-vivo methodology that is currently applied for tracking brain drug delivery devices. First we will focus on the most common labels and labeling procedures to detect and/or visualize brain drug delivery devices (living cells and nanocarriers). Subsequently, we will discuss specific applications in tracking drug delivery devices.

1. Introduction

Many potential drugs for the treatment of brain diseases show excellent in-vitro effects, but do not reach application in patients. The high failure rate of initially promising drug candidates is often caused by insufficient delivery of the drug into the brain, thus resulting in drug concentrations that are too low to be therapeutically effective [1]. There are two main administration routes to deliver a drug into the brain, i.e., by means of intracranial and intravascular administration. In the craniotomy-based route, a drug is administered via intracerebroventricular or intracerebral injection. However, major drawbacks of these approaches are invasiveness of this method and the limited penetration of drug from the injection site toward surrounding brain tissue. Even when the delivery of the drug is facilitated by nanocarriers, the drug-penetrated tissue area is rather small in case of intracranial injection. Consequently, this kind of procedure is only suitable for treatment of brain disorders that are confined to a specific region within the brain, such as in primary brain tumors, stroke, and Parkinson's disease [2,

3]. On the other hand, brain delivery of drugs via the vascular route is much more advantageous and therefore offers greater potential. This approach is much more patient-friendly and, once transported over the blood-brain barrier (BBB), the intravenously administered drug can literally reach every neuron in the brain [4]. However, delivery of drugs from blood into brain is often hampered by poor penetration of the BBB, especially in case of delivery of hydrophilic and macromolecular drugs.

The BBB consists of highly polarized endothelial cells supported by a basal lamina, pericytes, and astrocytic end feet [5]. Tight junctions between the endothelial cells separate their plasma membranes into apical (or luminal, facing the blood) and basolateral (or abluminal, facing the brain parenchyma) domains and prevent extensive paracellular transport. At either domain different sets of transporter proteins, receptors and enzymes are expressed that enable protection of the brain from entry of foreign substances and at the same time allow essential metabolites, such as glucose and amino acids, to enter from blood into the brain.

2. Drug delivery (in)to the brain

Poor accumulation of a drug into the brain is a major hurdle in the development of drugs, aimed at treating diseases related to the central nervous system (CNS). Penetration of drugs into the brain could theoretically be enhanced by administration of higher doses of the drug, but this strategy, apart from economic considerations, would also increase the exposure of peripheral organs, thereby enhancing the potential risk of toxic side effects. Therefore, in order to reduce toxicity and increase treatment efficiency, different approaches to selectively increase drug accumulation in the brain have been developed [1]. The first strategy relies on the incorporation or encapsulation of the drug into brain-targeting nanocarriers. When a lipophilic drug has to be delivered, binding of the drug-loaded nanocarrier to brain endothelium will suffice, as molecular exchange between nanocarrier and apical surface will allow the drug to enter the brain via passive diffusion. In case of hydrophilic or macromolecular drugs (e.g. proteins, peptides, oligonucleotides), the nanocarrier itself needs to cross the BBB and release its contents once it reaches brain parenchyma. A second approach for improving drug delivery to the brain involves the use of living cells that are engineered to produce the pharmaceutical agent, which is secreted into the brain after cellular translocation across the BBB. This strategy primarily involves the use of (ex-vivo) genetically modified (neural) stem cells that display the potency to cross the BBB

2.1. Nanocarrier-mediated drug delivery

Nanocarriers are particulate systems with diameters varying between 1 to 1000 nm that are usually composed of lipids or polymers, containing a drug payload. Nanocarriers for drug delivery into the brain are usually vehicles, consisting of a membrane-like structure that encloses an aqueous core. The membrane is often composed of a genuine lipid bilayer (liposomes), but also forms when using amphiphilic synthetic block copolymers (polymersomes). Alternatively, nanocarriers without an aqueous core have been prepared, including solid lipid nanoparticles and solid polymeric nanoparticles. The potential of using nanocarriers, such as liposomes, polymersomes and solid-lipid nanoparticles as drug delivery devices for the brain has been extensively reviewed by Tiwari and Amiji [6]. Besides these artificial drug delivery devices, Alvarez-Erviti et al. recently reported the potential application of exosomes, i.e., vesicular structures of 40-80 nm produced by distinct cell types, as vehicles for siRNA delivery [7]. Intrinsically, nanocarriers do not selectively target to the brain. Accordingly, in order to improve brain accumulation, specific peptides or antibodies that selectively recognize endothelial cell surface receptors, capable of engaging into transcytotic transport mechanisms, can be coupled to the nanocarriers. In this manner, transport of the carrier across the BBB would thus be specifically facilitated, leading to an enhanced delivery of the drug into the brain. Of potential interest in this regard are transferrin or insulin, which are naturally transported across the BBB from blood into brain via receptor mediated transcytosis [8, 9]. Hence, nanocarriers specifically engineered in this manner, and displaying BBB transcytotic capacity following systemic administration, may hold great promise for the treatment of multifocal brain diseases, including brain metastases, multiple sclerosis, Alzheimer's disease, and amyotrophic lateral sclerosis [10].

2.2. Cell-based drug delivery

Many studies in animal models have shown that neural stem cells migrate to sites of brain injury caused by e.g. a tumor [11], neurodegeneration [12] or cerebral ischemia [13]. Therefore, in such cases an alternative strategy for drug delivery to the pathologic brain involves the use of stem cells, transduced with a therapeutic gene [14]. These engineered stem cells are either injected into a peripheral vein or directly transplanted into the brain by intracerebral or intraventricular injection. By administration via intravenous injection, the number of cells reaching the brain may be relatively small [11], because the first barrier the cells encounter is the capillary network of internal organs. Due to their relatively large diameter (approximately 15 μm), the cells become

particularly trapped in the capillaries of the lungs, which is known as the pulmonary first pass effect [15-17]. In addition to capillary trapping, an interaction of the administered cells with cells of the reticuloendothelial system likely also plays a role in cell trapping, particularly in liver and spleen [15]. However, it has also been shown that the first pass effect can be alleviated using vasodilators [17, 18]. Thus this stem cell-based approach would benefit by further exploring possibilities to optimize means that improve the number of stem cells that reach the brain upon intravascular administration. Moreover, prolonged secretion of a drug from (genetically engineered) stem cells in the brain may result in therapeutic levels of the drug. Administration via cerebral or ventricular injection allows the application of cells close to or at the site of injury, which improves the efficacy of delivery, albeit at the expense of safety.

3. Monitoring trafficking of drug delivery devices

To monitor the efficacy of delivery devices for CNS-destined drugs, physiological effects induced by the drug in the brain could be monitored as surrogate endpoints of drug concentration. Such indirect measurements of drug delivery efficiency, however, would be prone to many confounding factors and therefore is usually not very sensitive. A more insightful approach would be to measure directly the concentration of the nanocarrier, as a measure of transcytotic efficiency, or that of the drug, as a measure of delivery/release, inside the brain. Obviously, to determine brain delivery efficiency of the nanocarriers, an accurate analysis and quantification of their overall body distribution is essential and hence requires an adequate and sensitive methodology to track these devices. Here we will discuss several *in vivo* and *ex vivo* approaches that have been applied so far.

Ex vivo detection of drug delivery devices in brain involves the isolation of brain tissue followed by biochemical and/or microscopic analyses. Most frequently used *ex vivo* examination methods are biodistribution studies, autoradiography and fluorescence microscopy. In general, ex vivo detection is commonly applied in animal studies, although post mortem material of humans, made available by so-called Brainbanks, can occasionally also be used. With appropriate (immuno)histological labeling of brain tissue, the exact position of drug delivery devices relative to the different brain structures and cell types can be determined. Next to visualizing the position of drug delivery devices in brain, ex vivo detection methods allow for a quantitative measurement of the accumulation of delivery devices in brain. A major disadvantage of *ex vivo* detection methods is that the trafficking of the drug delivery devices, i.e., their flow in body fluids and transport across cellular barriers, cannot be monitored in a longitudinal fashion.

In vivo detection methods are noninvasive and therefore allow multiple imaging sessions that may provide information on the distribution of nanocarriers and their contents within living tissue over the time. For *in vivo* imaging of the trafficking of nanocarriers, it is required that the device is modified with a label that can be detected outside the body. Depending on the labeling technique, drug delivery devices can be tracked in vivo over several hours, when labeled with short-lived radioactive isotopes, up to several weeks or months, when labeled with magnetic beads or reporter genes. Dual labeling, i.e., labeling of the drug delivery device as well as the loaded drug enables assessing the in vivo fate of both the carrier and the drug and therefore provides information on delivery device integrity and concomitant drug release. Moreover, *in vivo* imaging helps to determine the optimal application route and dosing regimens of the therapeutics.
In the next sections, we will briefly discuss the most relevant noninvasive imaging methods currently applied for monitoring migration of drug delivery devices.

4. Noninvasive imaging methods

4.1. Magnetic Resonance Imaging (MRI)

MRI is a high-resolution imaging technique that provides excellent soft tissue contrast [19]. In MRI, nuclei in a magnetic field are excited to a high energy spin state by a radiofrequency pulse. When these nuclei return to their low energy spin state, the electromagnetic flux is measured and converted into images. Two types of MRI images can be acquired: T1 and T2-weighted MRI. T1-weighted MRI is based on the longitudinal (realignment) relaxation time of the excited nuclei, whereas T2-weighted MRI is based on the transverse (spin phase) relaxation time. The signal of both T1 and T2-weighted MRI depends on the interaction of the relaxating nucleus with its immediate environment. MRI usually measures the spin relaxation of protons present in water. However, other atoms like ^{13}C, ^{23}Na and ^{31}P can also be used for MRI, but these atoms generate a much weaker signal and are far less abundant *in vivo* than ^{1}H. To increase the specificity of MRI different contrast agents have been exploited. These contrast agents have also been applied to label cells and molecules of interest for *in vivo* tracking. Two classes of contrast agents can be distinguished: paramagnetic and super-paramagnetic. Paramagnetic contrast agents, usually gadolinium complexes, enhance the signal in T1-weighted MRI, whereas super-paramagnetic contrast agents like iron oxide particles reduce the T2 signal. Super-paramagnetic contrast agents generally generate a stronger signal than gadolinium and are therefore often more sensitive.

4.2. Optical imaging

Among the most widely applied optical imaging techniques used today are fluorescence and bioluminescence imaging [20-22]. In fluorescence imaging, an external light source excites a fluorescent imaging probe inside an animal to a higher energy state. The fluorescent reporter probe subsequently returns to its ground energy state by emission of light with a longer wavelength [22]. The emitted light is detected outside the animal by a light sensitive camera. When multiple fluorescent probes are used that emit light at different wavelengths, various processes can be studied simultaneously using appropriate light filters. The major limitations of fluorescence imaging are the contribution of autofluorescence, which reduces the resolution of the probe, and poor penetration of light through tissue. Classical fluorescent probes like green fluorescent protein (GFP) emit light in the visible spectrum (400 – 650 nm) that is highly attenuated by haemoglobin and other proteins. Consequently only superficial targets (<1 cm deep) can be imaged with these probes. To overcome this problem, new probes that absorb and emit light in the near-infrared (NIR) region (700-1000 nm) and quantum dots (semiconductor nanocrystals) have been developed for fluorescence imaging [23]. Yet, fluorescence imaging is mainly suitable for application in small animals. Two-dimensional optical images preferentially show superficial activity and cannot resolve depth. The nonlinear attenuation of light by tissue makes quantification of optical imaging data a complicated task. Tomographic optical imaging devices have now been developed to overcome these limitations [24]. Improved quantification and volumetric localization can be achieved using transmission images that can be generated with light source-detector pairs at multiple angles [25].

In bioluminescence imaging [26], animals or specific cells have been engineered to express a light-producing enzyme (luciferase). Firefly luciferase is the most frequently used enzyme for bioluminescence imaging. In the presence of oxygen and adenosine triphosphate, firefly luciferase oxidizes its substrate luciferin, and produces yellow-green light with an emission peak of approximately 560 nm. Luciferases of other species, such as click beetle, and luciferases that react with different substrates, such as sea pansy (Renilla) and marine copepod (Gaussia), have also been used. Bioluminescence of firefly luciferase generates an emission spectrum of which about 30% is above 600 nm. Although a major portion of the light signal is absorbed and scattered by tissue, the low background associated with bioluminescence makes this technique more sensitive than fluorescence imaging.

4.3. Nuclear imaging

Positron emission tomography (PET) and single photon emission computed tomography (SPECT) are nuclear imaging techniques that can provide functional information about biochemical and physiological processes. Both PET and SPECT imaging are based on the detection of radiation emitted by an intravenously injected radioactive tracer using a dedicated camera [27, 28]. PET and SPECT differ in the radionuclide that is employed to label the tracer and in the detection technology of the camera.

PET isotopes, such as ^{11}C, ^{18}F and ^{89}Zr, decay by emission of a positron, which travels a short distance in tissue. When the positron has lost most of its energy, it annihilates together with an electron, resulting in the formation of two 511 keV photons. These photons are emitted at an angle of 180^{o} and are detected outside the body by the PET camera. PET is highly sensitive, as detection sensitivity is in the pico-molar concentration range. In PET, absorption of radiation by the body can be compensated for by attenuation correction, using a transmission scan that is made with an external radioactive source or a CT scan (for hybrid systems). A major advantage of PET over other imaging techniques is that it allows absolute quantification of the biochemical parameter of interest by pharmacokinetic modeling.

SPECT imaging uses probes that are labeled with radionuclides that emit single photons, such as ^{99m}Tc, ^{111}In and ^{123}I. For localization of the origin of the photons, a collimator is placed between the subject and the detector system. A collimator is a perforated plate - usually lead or tungsten - that can only be penetrated by photons that travel in the same direction as the channels in the collimator. Because the collimator blocks most photons, the sensitivity of SPECT is about 2 orders of magnitude lower than that of PET. In most systems, the collimator and detector rotate around the subject in order to obtain data in three dimensions. Quantification of SPECT data is a major technological challenge [29]. However, attenuation correction can be easily performed using an external radiation source or by acquiring a CT scan, followed by post-processing of the SPECT images, whereas methods for scatter correction are still in development. Because of the low sensitivity of SPECT, the count rate of the system may limit the temporal resolution for dynamic imaging. Nevertheless, in contrast to PET, multiple energy windows can be used in SPECT, which allows simultaneous imaging of different tracers labeled with different isotopes.

5. Labeling methods

Since drug delivery devices generally do not display intrinsic properties that allow their *ex vivo* detection or *in vivo* imaging, it is usually necessary to tag the drug carriers with a suitable label to enable tracking of their *in vivo* distribution. Depending on the detection or imaging tool used, several labeling methods are available. The selection of imaging technique and the labeling method strongly depends on the specific question addressed. Before discussing specific applications, we will first briefly highlight the most common procedures to label delivery vehicles– being either cell-based or artificial nanocarriers – as applied in brain delivery.

5.1. Direct labeling methods for cell-based drug delivery devices

5.1.1. Cell labeling with MRI contrast agents: Gadolinium complexes

Two major classes of MRI contrast agents have been used for tracking cells in the brain: gadolinium complexes and super-paramagnetic iron oxide particles.
Gadolinium is frequently used as a positive MRI contrast agent. Positive contrast agents cause a reduction in the T1 relaxation time, resulting in increased signal intensity on T1-weighted images, (i.e. appearing brighter on MRI scans). However, recent studies showed that gadolinium based contrast agents could give either positive or negative changes in MRI signals, depending on the specific localization of the contrast agent inside the cell. In particular, gadolinium that is dispersed throughout the cell cytoplasm leads to a decrease in the T1 relaxation time (positive MRI contrast), while gadolinium that is confined to endosomes leads to a decrease in the T2 relaxation time (negative MRI contrast) [30]. For the purpose of cell tracking in the brain, neural stem cells have been labeled with various gadolinium-based contrast agents, such as gadolinium-diethylene triamine pentaacetic acid (Gd-DTPA) and gadopentetate dimeglumine [31, 32]. After labeling, more than 90% of the stem cells were still viable, as determined by a Trypan blue exclusion assay. The Gd-DTPA label could still be detected in the stem cells in vitro for up to 2 weeks after labeling. Modo et al. labeled immortalized stem cells with a bimodal fluorescent MRI contrast agent, called gadolinium rhodamine dextran (GRID), consisting of rhodamine and gadolinium-DTPA chelates that are covalently attached to a 10 kDa dextran molecule [33]. Cell viability in the presence of GRID was largely unaffected. However, cell division resulted in a dilution of the GRID signal and as a consequence, the rhodamine signal could not detected anymore at day 7 after labeling, while the gadolinium signal allowed for detection of cell migration by MRI for up to 14 days after grafting in a rat middle cerebral artery occlusion model [34]. These results likely reflect the differences

in intrinsic sensitivities of the detection techniques. Giesel et al. showed that primary human mesenchymal stem cells can be readily labeled with Gadofluorine M, a macrocyclic gadolinium-based contrast agent with a perfluorinated sidechain. *In vitro*, the label was detectable inside the cells for an impressive period of 6 weeks. [35]. However, in this study important data on cell proliferation and cell viability are lacking.

5.1.2. Cell labeling with MRI contrast agents: Iron oxide particles

Iron oxide is frequently used as a negative contrast agent. Negative contrast agents predominantly produce reduction in T2 relaxation time, appearing dark on MRI scans. Super-paramagnetic iron oxide (SPIO) particles consist of a crystalline iron oxide core and a shell of hydrophilic polymer. There are two types of contrast agents based on super-paramagnetic iron oxides that are in clinical trials or already FDA approved: Feridex, which is a super-paramagnetic iron oxide colloid with a mean diameter of 150 nm (120-180 nm) and Sinerem, an ultra-small SPIO (USPIO) colloid with a mean diameter of 40 nm. Under normal conditions, these iron oxide particles can be taken up by cells via endocytosis. However, undifferentiated (stem) or less differentiated (progenitor) cells do not have the full endocytic capacity that is necessary for an efficient intracellular accumulation of iron oxide particles. To overcome this problem, the internalization of iron oxide particles by these cells has been improved by employing technologies developed for DNA transfection, such as the use of the commercially available delivery agents Lipofectamine, poly-L-lysine, protamine sulfate, Metafectene, JetPEI and Fugene [36, 37], Stojanov, unpublished). Application of these agents to assist cellular internalization of SPIOs resulted in labeled cells that could be detected *in vitro* by MRI for up to seven doubling cycles after labeling [37], and *in vivo* for at least 3 weeks [38, 39]. Arbab et al. have shown in human mesenchymal stem cells that the ratio of SPIO to delivery agent and the total amount of iron in the medium is critical for the efficiency of delivery of the total amount of iron into the cells [40]. When D3 embryonic stem cells and C17.2 neural stem cells were labeled with the USPIO Sinerem, the label was stably incorporated in both cell lines [37]. Interestingly, D3 embryonic stem cells showed to be less tolerant to high concentration of the transfection agent Metafectene. The general conclusion about cell labeling with iron oxide particles is that labeling protocols have to be optimized in a cell dependent manner for each combination of iron oxide particle and delivery agent [41]41) in order to optimize a balance between delivery efficiency versus toxicity [36]. In essence, this is in line with the cell-type sensitivity in terms of toxicity and efficiency, when applying distinct delivery devices in transfection studies.

Electroporation represents an alternative method to improve particle internalization by cells. Walczak et al., showed that when appropriate electroporation settings are used sufficient amounts of Feridex (Endorem) can be incorporated into C17.2 neural stem cells for in vivo imaging [42]. Using optimized conditions, cell viability and differentiation capacity *in vitro*, and proliferation and migration of the cells *in vivo* were maintained. As Feridex is an FDA-approved agent this method can be readily translated into a clinical setting.

Iron oxide particles in the micrometer size range were also suggested as possible contrast agents. In this case, the high amount of iron present in one particle gives a detectable signal, which allows for single particle imaging [43]. The size of the particle, however, can strongly influence the stability of the label in a proliferating cell population. Hinds showed that 0.9 μm iron oxide particles were evenly distributed between daughter cells of labeled mesenchymal cells [44]. On the other hand, 1.6 μm particles showed a tendency to be secreted by cells after long-term culturing and, in addition, led to uneven distribution of the label between daughter cells, leaving some of the cells without contrast agent [37]. Similarly as noted for the SPIO and USPIO particles, the use of these larger iron particles for cell labeling has to be validated for each cell type.

5.1.3. Cell labeling with fluorescent probes: Quantum dots

Semiconductor nanocrystals (quantum dots) are a new class of fluorescent probes with high quantum yield and resistance to photobleaching. Quantum dots (QDs) are characterized by size dependent absorption and emission. An emission wavelength range from 400 to 1350 nm is covered with QDs that are 2-9.5 nm in diameter [45]. The final size of QDs depends on the type of coating and functionalization. Cells can be labeled with QDs via spontaneous internalization. Similar as for iron oxide particles, QDs labeling efficiency can be improved by electroporation and conjunction with compounds employed in DNA delivery like cationic lipids or polymers. In addition, the use of a specific targeting peptide has been described to improve QD cell labeling efficiencies [45]. Lin et al. [46] labeled ES-D3 murine embryonic stem cells with peptide based QTracker. Flow cytometry showed that 72 % of the cells contained QDs 24h after labeling, whereas only 4 % of the cells remained positive at day 4. The authors argued that the loss of signal could be a consequence of fast cell division and/or active secretion of QDs from the cells. In vivo, the signal could be visualized for up to 14 days after subcutaneous administration of the labeled cells. However, histological analysis revealed that QDs were present in surrounding host cells instead of in teratomas that had grown from the embryonic stem cells. This finding suggests

that QDs were secreted from embryonic stem cells and subsequently taken up by neighboring host cells. As such, the determination of the stability of a trapping of a label inside the cell in an *in vitro* assay provides essential information on the feasibility of using that specific label for long term cell tracking *in vivo*.

Similar to any other fluorescent probe, QDs have to be excited by external light in order to emit the fluorescent light. However, external irradiation used in *in vivo* fluorescent imaging excites not only the artificially introduced fluorophore, but also endogenous fluorophores resulting in the production of high background fluorescence, i.e. autofluorescence (see below). Moreover, light will be absorbed and scattered by tissues leading to inefficient excitation of the fluorescent label particularly when present in deep tissue. In order to overcome these drawbacks of *in vivo* fluorescent imaging So et al. designed QDs that do not require external light for activation [47]. The group exploited a process called bioluminescence resonance transfer energy (BRET). In this approach, Luc8 luciferase was coupled to QD655 (QD with an emission wavelength of 655 nm). When the substrate coelenterazine is added, luciferase emits light with a peak intensity at 480 nm, which can excite QD655. The quantum dot will subsequently emit light at 655 nm. BRET emission (at 655 nm) is more readily detected than luciferase emission, particularly in deep tissues. Indeed, C6 glioma cells that are labeled with QD655-Luc8 could be visualized in lungs by application of the BRET technology, but not by fluorescence. It has been shown that native coelenterazine is a substrate for the efflux pump P-glycoprotein (ABCB1) that is abundantly expressed at the BBB. Therefore, application of the QD655-Luc8 construct for tracking cells in the intact brain may be possible only after administration of a P-glycoprotein inhibitor, such us GF120918 [48].

5.1.4. Cell labeling with radioactive probes: PET tracers

The glucose analogue 2'-[^{18}F]fluoro-2'-deoxyglucose ([^{18}F]FDG) is a widely available and extensively used PET tracer. [^{18}F]FDG enters the cell via GLUT transporters and is subsequently phosphorylated by hexokinase. [^{18}F]FDG 6-phosphate no longer permeates across the cell membrane and remains therefore trapped inside the cell. With a half-life of 110 minutes, [^{18}F]FDG can be used only for short-term cell tracking (4-6 hours). [^{18}F]FDG does not induce long-term radiotoxicity [49]. However, it has been shown that efflux of [^{18}F]FDG from stem cells is significant over time [17, 49]. This efflux is probably due to dephosphorylation of [^{18}F]FDG 6-phosphate by glucose phosphorylase, followed by release of free [^{18}F]FDG. Substantial efflux of the radiopharmaceutical was also found from human activated T lymphocytes [50] and rat C6 glioma cells [51]. *In vivo* released [^{18}F]FDG can be taken up by various tissues with

a high glucose metabolism, which result in a high background signal. We have shown *in vitro* that the efflux of [^{18}F]FDG can be partly inhibited by the glucose transporter inhibitor phloretin [17]. *In vivo*, however, a bolus administration of this GLUT inhibitor could not completely prevent loss of radioactive tracer from the labeled cells. Possibly infusion of phloretin, instead of a bolus injection, may further improve tracer retention inside the cells.

An alternative labeling method for short term cell tracking with PET is labeling of the cells with hexadecyl-4-[^{18}F]fluorobenzoate ([^{18}F]HFB). [^{18}F]HFB was used for labeling of mesenchymal stem cells by intercalation of the tracer in the cell membrane [52]. More than 90% of the incorporated [^{18}F]HFB was retained in the cells 4h after labeling, compared to only 60% for [^{18}F]FDG [49]. Accordingly, [^{18}F]HFB, although not commercially available, seems to be a more reliable and hence more appropriate tool for short term tracking of cells with PET than [^{18}F]FDG.

An alternative PET tracer suggested for cell tracking over a period of 24-36h is [^{64}Cu]pyruvaldehyde-bis-(N4-methyl-thiosemicarbazone) ([^{64}Cu]PTSM; half-life 12.7h) [51]. However, as for [^{18}F]FDG, significant efflux of radioactivity was observed over time for a variety of cell types tested [51, 53, 54]. For the same purpose ^{64}Cu labeled human leukocytes have been employed, using the membrane-permeable divalent chelator 2-(2-amino-4-methyl-5-flurophenoxy)methyl-8-aminoquinoline-N,N,N′,N′-tetra-acetic acid in combination with [^{64}Cu]tropolone. This method gives high labeling efficiency and 80% retention 24h after labeling. Attempts to label stem cells using this technique have not been reported yet.

5.1.5. Cell labeling with radioactive probes: SPECT tracers

Most commonly used SPECT radioisotopes are technetium-99m (^{99m}Tc, half-life 6h) and indium-111 (^{111}In, half-life 2.8 days). ^{99m}Tc-exametazime ([^{99m}Tc]HMPAO) is the radiopharmaceutical of choice for leukocyte labeling. It allows tracking of labeled cells up to 24 hours. The extent of spontaneous release of [^{99m}Tc]HMPAO depends on the cell type. For example, 2h after labeling there is no significant release of radioactivity from [^{99m}Tc]HMPAO labeled lymphocytes. In contrast, there is 19 % release of radioactivity from labeled polymorphonuclear cells during this period [55]. Only few attempts to radiolabel cells other than blood cells with [^{99m}Tc]HMPAO have been described thus far. In endothelial cells, a high labeling efficiency can be attained (10 MBq/10^6 cells) without any adverse effect on cell viability [56]. However, radioactive leakage was as high as 30% at 3h and 57 % at 18 h after labeling. We labeled murine C17.2 neural stem cells with [^{99m}Tc]HMPAO at a concentration of 5 MBq/10^6 cells without any sign of acute toxicity. However, leakage of radioactivity from the stem

cells was about 20% after 2h (unpublished data). Also mesenchymal stem cells have been labeled with [^{99m}Tc]HMPAO [57]. Although no labeling details were provided, release of ^{99m}Tc from these cells apparently also occurred, as can be inferred from the high radioactivity that was measured in the kidney and bladder. Since ^{99m}Tc that is released from the cells is excreted mostly via kidneys and intestine, leaving low background in the other tissues, [^{99m}Tc]HMPAO labeled cells may still be used for early stem cell tracking despite some leakage of radioactivity. However, proper control experiments should be conducted to discriminate whether the observed radioactivity in an organ originates from intact labeled cells, or from released ^{99m}Tc.

Next to [^{99m}Tc]HMPAO, [^{111}In]oxine has frequently been used for leukocyte radiolabeling. With a half life of 2.8 days, [^{111}In]oxine labeling should in theory allow the monitoring of cell distribution for over a week. [^{111}In]oxine was also used for labeling of several types of progenitor cells, but with various degrees of success. Murine hematopoietic progenitor cells proved to be sensitive to labeling with [^{111}In]oxine, as significant toxicity was observed when either 1 MBq or 0.1 MBq of tracer was applied per million cells [58]. A maximum dose of 0.14 MBq/10^6 cells has been reported that does not affect canine bone marrow-derived mesenchymal stem cell survival and function [59]. On the other hand, it has also been reported that human mesenchymal stem cells could be labeled with 7.5 MBq/10^6 cells without affecting the doubling time and differentiation into endothelial cells [60]. Human endothelial cells could even be labeled with [^{111}In]oxine at a concentration of 10 MBq/10^6 cells without changing viability or migration capacity [61]. In contrast, the same group also observed that labeling of human hematopoietic progenitor cells with a similar dose of [^{111}In]oxine abolished cell viability and differentiation 7 days later [62]. Thus, there appears to be a strong variability in sensitivity towards [^{111}In]oxine between cell types, with a tendency of a higher sensitivity for less differentiated cells. The mechanisms of cell damage have not been revealed yet, but probably include heavy metal poisoning, high radiosensitivity of cell lines, and cell handling during the labeling procedure [62, 63]. Besides the cellular toxicity of certain SPECT tracers, loss of radiolabel is another problem that poses limits to the detection time. For example, cellular retention of [^{111}In]indium 48 h after labeling of dendritic cells, and hematopoietic and endothelial progenitor cells ranges from 18 to 39% [58, 61, 64] depending on cell type and experimental settings. Due to this low retention, these [^{111}In]oxine labeled cells only provide reliable data for imaging up till 48h hours after labeling. Thus direct cell radiolabeling allows for short-term real time cell tracking. Despite the efflux of many radiotracers, direct radiolabeling of cells still allows for a comparative analysis of the availability of cells at the target site, for example, following different routes of administration.

5.2. Reporter gene-mediated labeling methods for cell-based drug delivery devices

Besides direct labeling of the cells, monitoring of cell trafficking can also be accomplished by introducing a so-called reporter gene within the cell of interest. Thus a reporter gene can be co-expressed together with a therapeutic gene in order to monitor cell migration and while applying gene therapy. Products of reporter genes can be directly detected (e.g. a produced fluorescent protein) or by functional assays in case the reporter gene leads to the expression of receptors, transporters or enzymes, which involves indirect means of detection. In the latter case an external probe has to be introduced in order to 'sense' reporter gene expression. When stably incorporated into the cell genome, reporter genes can in principle be continuously expressed and therefore they can be detected perpetually. In sharp contrast, transient transfection will result in loss of signal over time, because of dilution of the gene product during subsequent rounds of cell division. However, it has been noticed that, even in case of stable transfection, expression of reporter genes in stem cells can be silenced over time, which is usually caused by promoter methylation [65].

5.2.1. Reporter genes for MRI

A novel and emerging class of reporter genes are those that rely on detection by MRI [66]. For brain imaging, particularly the iron-based MRI reporter genes are of interest. An excess of iron inside the cell is stored by the iron storage protein ferritin. Recently, it was shown that ferritin overexpression in cells leads to an increased but non-toxic iron accumulation that is sufficient for noninvasive imaging [67, 68]. Furthermore, Zurkiya et al. investigated the magnetotactic bacterial gene, MagA, that is coding for the H^+/Fe(II) antiporter [69, 70] and responsible for the formation of SPIO-like nanoparticles within cells [71]. Magnetotactic bacteria are Gram-negative bacteria that produce intracellular magnetic structures composed of large amounts of iron, so-called magnetosomes, [72]. Although the magnetosome production in bacteria is probably controlled by multiple genes, MagA expression in the human embryonic kidney cell line 293FT resulted in the intracellular formation of nontoxic magnetic nanoparticles. Of particular interest, the presence of MagA-transfected cells could be detected by MRI *in vivo* following their implantation in the brain [71].

5.2.2. Reporter genes for fluorescence imaging

Fluorescent proteins are probably the most frequently used reporters. For in vitro use, variants of fluorescent proteins with emission wavelengths in the visible spectrum (400-600nm), such as green fluorescent protein (GFP) and red fluorescent protein (RFP), were developed (Table 1).

Table 1. Optical characteristics of fluorescent proteins suitable for in vivo application compared to GFP. Modified from: Deliolanis et al, 2008 [73].

Protein (Acronym)	Excitation Maximum (nm)	Emission Maximum (nm)	Molar Extinction Coefficient	Quantum Yield	Relative Brightness (% of EGFP)	ref
EGFP	489	509	53	0.60	100	[74]
tdTomato (Tandem)	554	581	138	0.69	283	[75]
mCherry	587	610	72	0.22	47	[75]
mRaspberry	598	625	86	0.15	38	[76]
mRFP	584	607	50	0.25	37	[75]
mPlum	590	649	41	0.10	12	[76]
Katushka	588	635	65	0.34	62	[77]

However, as noted above, visualization of fluorescent proteins *in vivo* is hampered by tissue autofluorescence. Molecules, such as flavins, collagen and elastin show natural fluorescence [78]. Excited in blue or green wavelengths these molecules emit throughout the visible wavelength range. Moreover, due to strong tissue (hemoglobin) absorption of light with wavelengths below 600 nm, most of the fluorescent proteins that have been designed for *in vitro* use cannot be used for cell tracking *in vivo*. Therefore, fluorescent probes that emit light with wavelengths between 600 nm and 900 nm, i.e., in the near-infrared range, are preferred for *in vivo* imaging [79]. Above 900 nm, light absorption by water molecules begins to interfere. However, over the past 10 years several red and near-infrared emitting proteins, suitable for *in vivo* application, have been developed (see Table 1, refs 75-77).

5.2.3. Reporter genes for bioluminescence imaging

In bioluminescence imaging, light generated by a chemical reaction between a substrate (external probe) and an enzyme (luciferase) is detected by an external camera. In order to reduce the tissue absorption and scatter observed in *in vivo* imaging,

luciferases with bioluminescence above 600 nm are preferred. Up to now, firefly luciferase (Table 2) is the most frequently used luciferase, because it emits light in this range.

Table 2. Properties of bioluminescent reporter proteins

Luciferase	**Species**	**Substrate**	**Peak emission wavelength (nm)**	**NB**	**ref**
Firefly	*Photinus pyralis*	D-luciferin	562 (550-620*)	* Mutants with various emission maximums exist	[80, 81*]
Click beetle	*Pyrophorus plagiophthalamus*	D-luciferin	546, 560, 578, 593		[82]
Renilla	*Renilla reniformas*	Coelenterazine	480, 547		[83, 84]
Gaussia	*Gaussia princeps*	Coelenterazine	480	Naturally secreted. Probably restricted passage across the BBB [85]	[86]
Bacterial luciferase	Photorhabdus luminescens	Endogenously produced	490	codon-optimized for expression in human cell lines	[87]

In contrast to fluorescent probes, luciferases do not require excitation by an external light source. As tissues do not show auto-emission of significant amounts of light, bioluminescence is generally characterized by a lower background signal than fluorescence. An overview of the various applications, advantages and disadvantages of the use of luciferases in vivo are reviewed elsewhere [81, 88].

Due to tissue attenuation and light scattering, bioluminescence imaging does not allow absolute quantification of the signal. Moreover, for brain imaging one should keep in mind that luciferin (firefly and click beetle luciferase substrate) and coelenterazine (Renilla and Gaussia luciferase substrate) are recognized by the ABC transporters ABCG2 and ABCB1, respectively, that are both expressed at the BBB [48, 89].

Consequently, substrate kinetics in the brain may differ from kinetics in peripheral tissues. Some bacteria produce luciferases that could be interesting for bioluminescence imaging in the brain. In contrast to eukaryotic luciferases that are encoded by one gene, bacterial luciferases are coded by a cassette of 5 genes, the Lux operon. While a luciferase dimer is encoded by genes luxA and luxB, the other three genes (luxCDE) encode for the required enzyme substrate [90]. Since both luciferase and its substrate are the product from the same operon, external application of the substrate is not required. This feature of the Lux operon makes it highly attractive for cell tracking in the brain. Recently stable expression of the codon-optimized Lux operon in the human HEK293 cell line has been reported [87]. However, the potential of this expression system in brain research remains to be explored.

5.2.4. Reporter genes for nuclear imaging

Many PET and SPECT reporter probes (Table 3) have been developed over the past years [91]. However most of them fail to cross the intact BBB. On the other hand probes that can cross the BBB, such as probes for the D2 receptor, give a high background signal in the brain, due to the presence of endogenous target receptors.
Recently the first PET reporter system for imaging gene expression behind the intact BBB has been introduced [99]. For that purpose, $hCB_2(D80N)$, a human gene encoding the cannabinoid receptor-2 which is deficient for signal transduction, has been exploited. CB_2 has low endogenous brain expression. Brain adenoviral overexpression of $hCB_2(D80N)$ was visualized using [^{11}C]GW405833, a CB2-selective partial agonist that crosses the BBB. Nevertheless, the potential to use this system for stem cell tracking in the brain [100] requires further investigations. In fact, a potentially perturbing factor in applying this reporter gene system is that expression of CB_2 is upregulated by activated microglia during inflammation. Since many brain disorders are accompanied by activation of microglia, it might therefore be difficult to discriminate between cell migration *versus* microglia activation, using this reporter gene at disease conditions.

Table 3. Available PET and SPECT reporter genes.

Reporter gene	Reporter probe	Radioisotope	Reporter probe crosses intact BBB	NB	ref
Herpes simplex virus type-1 thymidine kinase (HSV1-tk)	Various pyrimidine and acycloguanosine derivatives	^{11}C, ^{18}F, ^{124}I, ^{131}I – PET ^{123}I, ^{125}I - SPECT	no		[92]
Dopamine D_2 receptor (D_2R)	Fluoroethylspiperone (FESP)	^{18}F - PET	yes	Large background signal in the striatum	[93]
Dopamine transporter (DAT)	TRODAT-1	^{99m}Tc -SPECT	yes	Large background signal in the striatum	[94]
Sodium-iodide symporter (NIS)		^{99m}Tc-pertechnetate, ^{125}I - SPECT	no		[95]
Somatostatin receptor	Octreotide P2045 P829	^{111}In - SPECT ^{99m}Tc - SPECT	no		[96, 97]
E.coli xanthine phosphoribosyltransferase (XPRT)	Xanthine		yes	Unavailable radiolabeled reported probe	[98]
Human cannabinoid receptor 2 deficient for signal transduction $hCB_2(D80N)$	GW405833	^{11}C – PET	yes	Background signal from activated microglia?	[99]

5.3. Labeling methods for nanocarriers as drug delivery devices

Liposomes are classical nanoparticulate drug delivery devices. Not surprisingly therefore, most of the labeling techniques have been developed for liposomes. Some of these techniques have later been adopted for labeling of other nanoparticles. Thus liposomes have been labeled for detection by means of the different imaging modalities, including MRI, optical imaging, and PET/SPECT. In principle, there are three approaches for liposome labeling. In the first approach, hydrophilic tracers are trapped in the aqueous core of the liposome, while lipophilic tracers become trapped within the lipid bilayer. In the second strategy, the tracer is covalently coupled to the liposomal membrane. The third approach involves non-covalent binding of the tracer to

a chelator that is subsequently covalently coupled to the membrane. The stability of labeled nanoparticles is usually examined *in vitro* by incubation in buffer and plasma for an extended period of time, followed by determination of the presence of free label and/or nanoparticle metabolites, using ITLC or column chromatography. However, due to dilution effects and shear stress in blood, variations in microenvironment, clearance (i.e. interaction with cells of reticuloendothelial system, renal and biliary clearance), *in vivo* stability of labeled nanoparticles may substantially differ from their stability observed *in vitro*.

5.3.1. Nanocarrier labeling with MRI contrast agents

Of all potential brain drug delivery devices, only liposomes have been labeled with gadolinium chelates to obtain MRI contrast. Gadolinium contrast agents can be incorporated into liposomes by several cycles of freeze-thawing followed by extrusion through filters in order to obtain liposomes of a homogeneous and well-defined size. In this way, gadolinium-DTPA, gadodiamide and gadoteridol have been incorporated in liposomes [101-103]. Alternatively, a gadolinium chelator such as DTPA has been covalently coupled to a lipid that is incorporated into the liposome bilayer [104]. Subsequent addition of gadolinium will then assure its binding to the liposomal surface via chelation by the DTPA-derivatized lipid analogue. Interestingly, localization of the gadolinium at the liposomal surface, compared to encapsulated gadolinium, results in an improved MRI signal, which was attributed to a stronger interaction of surface-localized gadolinium with surrounding water molecules [105]. However, a disadvantage of surface exposure of the bulky DTPA is that it may sterically hinder the interaction of the liposomes with target cells. Analogously, BBB penetration may be reduced by the polar metal complex at the surface of the carrier. Indeed, thus far no studies have been reported on the use of gadolinium labeled liposomes in brain delivery.

Preparation of iron-labeled liposomes, based on the encapsulation of iron oxide nanoparticles, has also been described [106, 107]. Recently, also polymersomes have been labeled with magnetic nanoparticles. Depending on the type of initial solvent for the polymer and nanoparticle mixture, magneto-polymersomes, i.e. polymersomes with a shell that is densely packed with nanoparticles, can be formed upon subsequent dilution in aqueous medium [108, 109]. Despite the interesting potential of these magnetic polymersomes, no data on brain drug delivery research using these iron-labeled nanocarriers has been reported so far.

5.3.2. Nanocarrier labeling with fluorescent probes

Liposomes and polymersomes can be readily labeled with lipophilic dyes, such as 6-coumarin, which become an integral part of the bilayer during liposome/polymersome formation [23, 110, 111]. Alternatively, fluorescent lipid analogs such as 1,1'-dioctadecyl-3,3,3',3'-tetramethylindocarbocyanine perchlorate (Dil) and N-(lissamine rhodamine-B sulfonyl)-phosphatidylethanolamine (N-Rh-PE) have been used to label liposomes prepared for in vivo application [112]. Moreover, new fluorescent lipids can be made by the esterification of fluorescent dyes with fatty alcohols. For example, Deissler et al. esterified carboxylic acid-modified DY-676 with stearyl alcohol. The DY-676-C_{18} ester was then applied in the preparation of stable near-infrared fluorescent liposomes [113]. Likewise, near-infrared Cy7.5 hydroxysuccinimide was used to label 1,2-dioleoyl-sn-glycero-3-phosphoethanolamine (DOPE) [114]. Cy7.5-DOPE containing liposomes were then used to visualize the targeting of liposomes to lung tumors. Many fluorescent dyes are available with several modifications, such as amino, carboxylic acid, maleimide and hydroxysuccinimide groups (for a review see [115]). These functional groups are generally applied for the conjugation of peptides and proteins, including antibodies. However, these functional groups make it also possible to label targeted liposomes, allowing monitoring of improved programmable delivery of the liposomes.

5.3.3. Nanocarrier labeling with radioactive probes

In order to efficiently entrap a radiotracer in the aqueous core of liposomes a trans-chelation method can be used [116]. During liposome preparation a strong lipophilic chelator such as DTPA is encapsulated. Subsequently, liposomes are incubated with a complex of a weak chelator and a radiotracer such as ^{111}In-oxine. ^{111}In-oxine can pass the lipid bilayer allowing trans-chelation of ^{111}In from the weak oxine complex to the strong DTPA complex. Unbound radiotracer can be removed by dialysis. For the purpose of binding of radiotracer to the surface of liposomes, DTPA-phosphatidylethanolamine (DTPA-PE) is incorporated into the lipid bilayer during liposome preparation [117]. Subsequent radiolabeling of the liposome preparation can be performed by trans-chelation as described above. However, it should be noted that chelators are usually highly charged and relatively bulky molecules. When exposed on the surface of liposomes they can therefore readily influence the interaction of the liposomes with the surface of target cells. Accordingly, when used for liposomal membrane labeling, chelators are typically used in trace amounts in order to minimize

their effect on liposome-target cell interactions. Overall, entrapment of the chelator-radiotracer complex is preferred over surface exposure of the complex. A recent review on methods for radioactive liposome labeling, describing examples for each labeling strategy, is presented in Phillips et al [118].

There are only few examples of radiolabeling of other nanoparticles that might be potentially used as drug carriers. Solid lipid nanoparticles have been successfully labeled with ^{64}Cu by incorporation of lipid-PEG-BAT, a conjugate between a synthetic pegylated lipid and the copper specific chelator, 6-[p-(bromoacetamido)benzyl]-1,4,8,11-tetraazacyclotetradecane-N,N',N'',N'''-tetraacetic acid (BAT), followed by complexation of the radiometal [119]. Their biodistribution was quantitatively evaluated both *in vivo* (using PET imaging) and *ex vivo* (by gamma counting). On the other hand Harivardhan Reddy et al. labeled an anti-cancer drug etoposide encapsulated in SLNs with [^{99m}Tc]technetium pertechnetate after reduction with stannous chloride, while Upadhyay et al. labeled polymersome loaded Docetaxel in the same way [120, 121]. The ^{99m}Tc labeling was shown to be stable both in vitro and in vivo and allowed successful pharmacokinetics and biodistribution studies.

6. *Ex* vivo analysis of drug delivery device distribution

6.1. Ex vivo biodistribution

Upon systemic administration of radiolabeled cells or nanocarriers, *ex vivo* biodistribution studies are usually done to determine the fraction of the injected dose that accumulates into the brain. To this end, animals are sacrificed at specific time points after administration of the labeled device, relevant tissues are excised, and radioactivity is determined in the various samples. Recently, a quantitative procedure for determining tissue distribution of nanoparticles, using iron oxide labeled nanoparticles in conjunction with electron spin resonance spectroscopy, has been described [122]. In addition, the pharmacokinetics of drug-loaded nanocarriers can be determined by measurement of the drug concentrations in blood samples, taken at multiple time points. In this manner, tissue influx and efflux rate constants can be calculated. This procedure is similar to pharmacokinetic studies of the free drug [123].

Brain accumulation of (non)targeted nanoparticles is typically low compared to the total injected dose, but appears highly variable when different nanoparticles are compared. For example, two hours after i.v. administration of poly(ethyleneglycol)-poly(ε-caprolactone) polymersomes coupled with OX26 antibodies to target vascular endothelial cells into rats, the amount of brain-localized polymersomes was only 0.14 % ID/g tissue [111]. Similarly, one hour after i.v. administration of nanoparticles

composed of a PEG-n-hexadecylcyanoacrylate block-copolymer, the concentration in mouse brain was ~0.2 % ID /g tissue, whereas in rat brain the fraction of the injected dose was only 0.005 % ID / g tissue. [124]. However, in case of nano-PEG-**cross**-PEI nanogels, the fraction within the brain 1h after i.v. injection in mice reached as high as 2.67% ID/g tissue [125]. The high variability of brain accumulation of nanoparticles cannot only be ascribed to intrinsic differences between the nanoparticles and species under investigation, but also to differences between experimental protocols, such as time points of sampling after particle administration, and processing of the brain before particle quantification. For example, when nanoparticle accumulation is quantified for the whole brain, the presence of residual nanoparticles in capillary blood can significantly influence the results. It is therefore critical, prior to the isolation of the brain, to perfuse the organ with buffer to remove residual nanoparticles from the capillaries [23, 126-128]. Alternatively, total brain nanoparticle content can be corrected for the (estimated) blood volume and blood nanoparticle concentration [129, 130]. The need for such a correction is dictated by the assumption that the blood pool nanoparticle contribution in the total brain nanoparticle content should not exceed 10% and that the blood volume of the brain corresponds to approximately 12 µl/g of brain [131]. This would mean that the blood nanoparticle concentration should not exceed (10/100) / (12/1000) = 8 times the total brain concentration.

Generally, biodistribution studies provide information on the overall nanoparticle/drug accumulation in the brain. In order to discern between the accumulation of drugs in brain parenchyma and brain vasculature, Triguero et al. introduced the capillary depletion method [132]. For that purpose, the drug compound is radiolabeled and administered together with a marker compound that is labeled with another radiolabel and known to be retained within the vasculature. At the end of the experiment, the brain is isolated, homogenized, and centrifuged in a density gradient medium, usually containing dextran. Following centrifugation, the activity of both radiolabels is measured in the supernatant, serum and pellet fractions that represent parenchyma, blood, and capillaries, respectively. The volume of distribution (V_d) of the test compound in parenchyma and the capillaries can then be calculated. The percentage of contamination of the parenchyma with vascular tissue can be assessed by measurement of the specific activity of a vascular marker in the supernatant. Gutierezz et al. used gamma-glutamyl transpeptidase as a vascular marker and showed that in their experimental settings contamination of parenchyma with vasculature is approximately 2% [133]. On the other hand, Moos and Morgan used an assay for alkaline phosphatase (EC 3.1.3.1) and showed a contamination level of approximately 16% [8, 134]. Using this assay, Gosk et al. concluded that the accumulation of OX26-targeted liposomes in the parenchymal fraction was clearly a consequence of contamination with liposomes

from the capillary fraction. The finding was confirmed by confocal microscopy, which showed that liposomes accumulate in capillaries, but do not cross the BBB. Until now the brain accumulation of nanoparticles, both targeted and non-targeted, represents only a small fraction of the administered dose. Therefore methods such as capillary depletion and morphological examination are of crucial importance for determining genuine accumulation of nanoparticles into brain parenchyma.

6.2. Autoradiography

Autoradiography of radiolabeled drug delivery devices can be used to visualize *ex vivo* the regional distribution of such vehicles in the brain. Sakamoto and Ido [135] used autoradiography to compare the distribution of sulfatide-containing liposomes with size less than 100 nm in diameter in brain sections before and after unilateral osmotic opening of the BBB. Liposomes were administered via an internal carotid artery in order to achieve a high concentration of the liposomes in the brain. In case of an intact BBB, the distribution of the liposomes was confined to circumventricular organs, i.e. the pineal body and the regions around the third and lateral ventricles, with a similar distribution in the left and right hemisphere. For the purpose of osmotic opening of the BBB, a hypertonic mannitol solution was injected into the left carotid artery shortly before administration of the liposomes. At these conditions, the liposomes showed a homogenous distribution through the whole hemisphere subjected to osmotic opening of the BBB. The distribution of liposomes in the contralateral hemisphere was similar to that observed in case of an intact BBB. The resolution obtained by autoradiography is too low to discriminate between localization of liposomes in capillaries and brain parenchyma. However taking previous results into account it is very likely that upon opening of the BBB liposomes may distribute within brain parenchyma. In contrast to optical imaging where fixation and often staining of tissue is required, no post-processing of tissue is necessary for autoradiography. Although autoradiography is readily applicable and may provide quantitative insight about distribution of (non)targeted nanoparticles, the technology is currently not widely used in analyzing drug delivery into the brain.

6.3. Fluorescence microscopy

Fluorescence imaging is widely used in brain drug delivery research. Cells within the brain, labeled with quantum dots, fluorescent dyes, or expressing fluorescent proteins can be readily detected in tissue slices [11, 33, 136-138] by high resolution confocal imaging. This approach also allows to distinguish between brain parenchyma and

blood vessels, for example by (co-) visualizing specific markers of endothelial cells, such as CD31, using immunostaining [139, Georgieva, unpublished], see Figure 1.

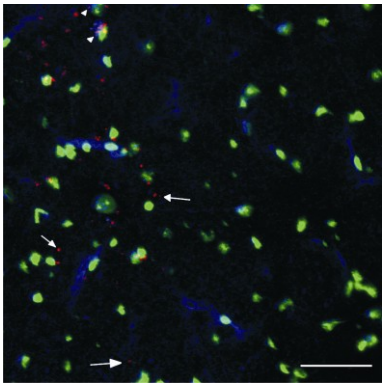

Figure 1. In vivo brain distribution of polymersomes after intracarotid artery injection. BALB/c mice were injected with G23-polymersomes. 24 hrs later the brains were isolated and processed for immunohistochemistry. (a) G23-polymersomes are found in microvessels, visualized by immunostaining for CD31 (PECAM), and in brain parenchyma. Polymersomes are pseudocolored in red, CD31 in blue and nuclei in green. Scale bar, 50 µm. (J.V. Georgieva et al; unpublished data)

Analogously, Gosk et al. stained brain slices for laminin and demonstrated in this manner that OX26-targeted liposomes, administered by in situ perfusion, were confined to brain endothelial cells, rather than penetrating brain tissue, since no co-localization was seen between the liposomes and laminin, which is a basal marker [134]. Similarly, the relative localization of nanoparticles with respect to glial cells and neurons can also be revealed by confocal microscopy, using appropriate markers for these cells [140].

In recent years, an interesting approach has been developed to monitor simultaneously fate and therapeutic efficacy of nanocarrier-mediated delivery. The approach, which relies on the use of dual and triple reporter genes, involves the preparation of a gene construct coding for one or two different reporter genes and/or a gene producing a therapeutic protein. In this manner insight is obtained, either in vivo or in vitro, into both cell distribution and expression of therapeutic genes. Following such a procedure, Tang et al. stably transfected C17.2 neural stem cells (NSCs) with a plasmid coding for both firefly luciferase (FL) and enhanced green fluorescent protein (eGFP) [11]. Bioluminescence was used to monitor the in vivo migration of C17.2 NSCs to glioblastomas in brain, while eGFP expression was used for histological confirmation *ex vivo* of the *in vivo* imaging results. The same combination of reporter genes can be used to monitor long-term lentiviral vector-mediated gene expression in brain [141].

7. In vivo imaging of drug delivery device trafficking

Several noninvasive imaging techniques have been applied to monitor trafficking of drug delivery devices. Due to the large tissue penetration depth of the imaging signal, PET, SPECT and MRI are applicable both in animals and in humans, making these approaches important tools in translational research. The resolution of optical imaging is relatively poor compared to PET, SPECT and MRI, and results are usually not quantitative due to tissue attenuation and scattering of light. However, *in vivo* bioluminescence and fluorescence imaging have been applied in small animal experiments because of simplicity and low costs [20]. Moreover, optical methods are ideally suited to bridge the gap between *in vitro* experiments and animal studies, as *in vivo* imaging results can be easily correlated with *ex vivo* microscopic analysis. Recent developments in optical imaging instrumentation enable interesting new applications in basic research, such as fluorescence tomography and intravital microscopy [20]. Although there are examples of using in vivo imaging techniques to track central nervous system drug delivery devices in humans [38, 142], this field is still in its infancy.

7.1. Tracking drug delivery devices by MRI

MHP36 stem cells have been labeled with gadolinium rhodamine dextran (GRID) for visualization by MRI. Following their engraftment in the contralateral hemisphere of rat brains with unilateral stroke damage, the spatial distribution and rate of migration of the GRID-labeled cells could be revealed [33, 34]. MRI demonstrated that 14 days after transplantation the labeled neural stem cells had migrated from the unaffected hemisphere along the corpus callosum to the peri-lesion area.

Similarly, rabbit neonatal NSCs have been labeled with Gd-DTPA in order to non-invasively follow the distribution and migration of cells after acute peripheral nerve traction injury [32]. Labeled cells were grafted on distracted sciatic nerves. Serial MRI for up to 70 days after transplantation showed sustained increases in T1 and T2 signals, which was accompanied by improved nerve regeneration. Since transplanted NSCs did not differentiate into neurons or Schwann cells during the time of the experiment, the observed nerve regeneration was attributed to neurotrophic factors released by NSCs.

The migration of Feridex-labeled C17.2 NSCs has been investigated using MRI after intraventricular transplantation in a shiverer mouse demyelination model [143]. It was possible to follow cell dissemination shortly after transplantation. In most animals the transplanted cells distributed homogenously throughout the ventricular system. Occasionally, the cells distributed to just one of the lateral ventricles. An interesting

finding was the observation of a mismatch between the cellular distribution, as visualized by MRI, and the histological examination, carried out at 6 days after stem cell transplantation. It was found that stem cells, heavily labeled with iron-oxide particles, remain in close proximity of the injection site, while cells that migrated further into the brain parenchyma contained lower amounts of Feridex. The authors investigated the release of the label from the cells *in vitro* and concluded that the loss of Feridex by stem cells was a consequence of asymmetric cell division and cell death. Accordingly, the conclusions appears justified that stem cell labeling with small iron oxide nanoparticles like Feridex, is not suitable for long-term tracking of proliferating cells.

Magnetic tumor targeting is a strategy to deliver drugs, carried by magnetic nanoparticles, into a tumor [144, 145]. It is known that tumor blood vessels show enhanced permeability and decreased blood flow [146]. Under these conditions, nanoparticles passively accumulate from blood into the tumor. In magnetic targeting, a strong magnet is placed on the body close to the tumor after intravenous administration of iron oxide nanoparticles, leading to a further increase of nanoparticle accumulation in the tumor. Typically, non-PEGylated magnetic nanoparticles are quickly cleared from circulation by the liver and the spleen, but their circulation half-life can be drastically increased upon PEGylation [147]. The extent of accumulation vs. clearance of PEGylated and non-PEGylated iron oxide nanoparticles has been examined over time by MRI in a rat 9L-glioma brain tumor model [147, 148]. The data revealed an increased accumulation into the tumor of PEGylated compared to non-PEGylated nanoparticles, which could be further promoted (approximately 5-fold) upon magnetic targeting of the iron oxide-loaded nanoparticles, as verified by *ex vivo* quantification. Moreover, overall, magnetic targeting proved to be more efficient for the PEGylated nanoparticles as they accumulated in the tumor at a concentration that was 15-fold higher than that observed for nanoparticles, devoid of the PEG coating.

Convection enhanced delivery (CED) is an experimental method developed in the early 1990s, by which a drug is delivered directly to the brain tumor through a cannula connected to an infusion pump [149]. The pump induces positive pressure, thereby dilating the tissue and allowing spreading of the drug. Various pump, catheter and cannula parameters have been incorporated in mathematical models in order to predict in vivo spreading of administered drug. Nevertheless, the success of the method is partly limited due to a lack of knowledge about the distribution of the drug *in situ*. Thus further validation of new and existing models requires careful tracking of the infused molecules *in vivo*. MRI with gadodiamide and fluorescently labeled liposomes has been applied to evaluate real time distribution and retention of liposomes after CED to rats, bearing a 9L-2 tumor [102]. In this manner it could be established that the

liposomal distribution within brain tissue, as measured by MRI, corresponded well with that observed by *ex vivo* fluorescence imaging. Interestingly, in these studies it was also demonstrated that the brain tissue distribution of the gadodiamide liposomes mimicked that of the (commercially available) liposomal drug Doxil. Therefore it was suggested [102] that gadodiamide labeled liposomes may serve as a useful marker for the brain tissue distribution of Doxil, administered via CED. Real-time MRI monitoring of liposomes loaded with Gadoteridol in combination with CED also provides opportunities for more accurate, site-directed delivery of drug-loaded liposomes to specific brain regions via online control of the administered dose. As the volume of distribution can be determined from the scans, MRI-monitored CED provides options for software development that could be used in predictable liposomal infusion in target structures [2, 103].

7.2. Tracking drug delivery devices by bioluminescence imaging

Bioluminescence has been used to compare different delivery methods of neuronal progenitor cells to brain tumors in mice [11]. To this end, firefly luciferase transfected C17.2 stem cells were injected into the intraperitoneal cavity, vasculature, ventricle or brain parenchyma. Bioluminescence imaging demonstrated migration of the cells from parenchyma or ventricle of the healthy hemisphere across the corpus callosum towards the tumor site. However, intravenous administration of the transfected cells resulted in only a modest migration towards the tumor, whereas tumor targeting was virtually absent after intraperitoneal administration.

Interestingly, when different luciferases with different light emission spectra are used, bioluminescence can also be applied to monitor two processes simultaneously. This approach has been employed for simultaneous monitoring of tumor growth, using glioma cells expressing Renilla luciferase, and migration of neural stem cells, expressing the secreted form of an apoptosis inducing ligand (S-TRAIL) and firefly luciferase [150]. In this manner it was shown that the NSCs, after administration to healthy brain, remain at the site of implantation where they proliferate [11]. In contrast, when implanted into the brain of the tumor-bearing mice, NSCs producing S-TRAIL migrate toward the glioma, and significantly reduce tumor growth [150]. Since bioluminescence only allows quantification of relative changes in the signal if the source of the signal remains at the same location in the body, it is not possible to determine whether NSCs proliferate during migration.

7.3. Tracking drug delivery devices by fluorescent molecular tomography

Planar fluorescence imaging is generally is not used for brain analysis, because the technique does not allow quantification of the signal due to a nonlinear dependence of signal intensity and tissue depth. In addition, planar fluorescence imaging suffers from poor sensitivity and spatial resolution because of tissue light absorption and scattering [25, 78]. However, fluorescence molecular tomography (FMT; [151], a three dimensional quantitative imaging technique, relying on the use of distinct fluorescent probes, has been successfully used in neuroimaging. Since FMT does not provide anatomical information, its combined use with a technique such as CT or MRI is preferable. According to this principle, FMT has been applied to track changes of protease activity during brain tumor growth and chemotherapy [152], employing ProSense680 as a fluorescent probe for revealing protease activity. Simultaneously, gadolinium enhanced MRI was carried out to visualize the anatomical structures and to calculate tumor volume. Interestingly, FMT showed changes of tumor protease activity early during chemotherapy, which disappeared at the end of chemotherapy, whereas MRI detected changes in tumor volume only in later stages of chemotherapy. Thus, the combined FMT-MRI imaging approach revealed early chemotherapeutic effects that properly reflected the predictive outcome on tumor response. Beta-amyloid plaques in a murine Alzheimer's disease model have also been analyzed by FMT, using the fluorescent dye oxazine [153]. By combining FMT with structural information as obtained by CT, the FMT reconstruction algorithm could be substantially improved, enabling far more precise signal localization, as subsequently confirmed by *ex vivo* imaging.

However, thus far FMT has not been used in studies on drug delivery into the brain. Yet, the principle of the approach, as highlighted by the work discussed in the preceding paragraph, offers a great potential for application in this field as well.

7.4. Tracking drug delivery devices by intravital confocal microscopy

Intravital two photon laser scanning microscopy is a highly invasive *in vivo* method that provides the best resolution of all *in vivo* imaging techniques, currently available. Intravital microscopy has been used to study events at the level of microvasculature. For that purpose, brain cortical microvasculature is exposed. For longitudinal imaging, a cranial window is inserted by removing a piece of scull and replacing it with glass [154]. Alternatively, a section of scull can be thinned using a combination of high speed drilling and scraping with a microsurgical blade [155]. A disadvantage of the latter method is that thinned bone grows back again. Thus, for longitudinal studies with

multiple imaging sessions, the bone has to be re-thinned. Recently, Drew et al. introduced a procedure to create a stable window in the scull by polished and reinforced thinning of the scull [156]. The major improvement of this technique compared to the method of Grutzendler is that upon thinning a cover glass was glued to the scull to prevent regrowth. In this way, good visibility was achieved for up to 3 months.

Multiphoton laser scanning microscopy in combination with intravital microscopy was used to analyze the influence of liposome composition on vascular accumulation in normal tissues and brain tumors [157]. Enhancement of the cationic charge of the liposomes resulted in their increased accumulation in tumor vessels, whereas no change in interstitial accumulation was observed. Dreher et al. developed a method to quantify tumor vasculature permeability of macromolecules by monitoring their fluorescence intensity in the vascular and extravascular space [158]. They showed that permeability of tumor vasculature was significantly more reduced for dextrans with increasing molecular weight. These studies suggest that confocal intravital microscopy has the potential of revealing whether targeted nanoparticles can cross intact BBB or at least that the drug, contained in the transport vehicles, gains access into the brain.

7.5. Tracking drug delivery devices by PET or SPECT

PET and SPECT imaging have been used for assessing the outcome of stem cell therapy. For example, [^{18}F]FDOPA PET was used to measure dopamine production in patients with Parkinson's disease, who had received embryonic dopamine cell implantation. One year after surgery, [^{18}F]FDOPA uptake was about 40% higher in patients that underwent transplantation than placebo treated patients. Increased tracer uptake correlated well with clinical symptoms, although primarily in case of patients of 60-years of age or younger [159]. Other examples of PET imaging for the indirect assessment of stem cell therapy efficacy have recently been reviewed by Wang et al. [160]. Apart from indirect monitoring of stem cells with PET or SPECT, only a few examples have been published of direct tracking of stem cells. Miletic et al. examined *in vivo* killing of 9L glioma cells by bone marrow derived stem cells, expressing the thymidine kinase of herpes simplex virus (HSV-tk) [137]. HSV-tk is used as suicide gene in cancer therapy, and phosphorylates antiviral prodrugs like ganciclovir and acyclovir. This phosphorylation of the prodrug triggers a chain of events that leads to the death of both the HSV-tk expressing cells and their neighboring cells [161]. Thus bone marrow–derived mesenchymal stem cells were injected into 9L tumors, followed by treatment of the animal with ganciclovir. Phosphorylated ganciclovir is produced in the stem cells, but can also be transferred from stem cells to glioma cells (bystander

effect). Apart from bringing about a therapeutic effect, HSV-tk expression in the stem cells can also be used as a reporter gene to localize stem cells *in vivo* by means of PET. To this end an HSV-tk-specific radioactive reporter probe, 9-[4-[^{18}F]fluoro-3-hydroxymethyl)butyl]guanine ([^{18}F]FHBG), is introduced, 6-7 days after intra-tumoral implantation of the stem cells. The drawback of the method is that [^{18}F]FHBG poorly penetrates the intact BBB, implying that visualization in the brain is possible only when the BBB is damaged, which often accompanies brain tumor development.
The biodistribution of ^{111}In-oxine-labeled human embryonic stem cell-derived neural progenitor cells and rat hippocampal progenitor cells was followed in rats with middle cerebral artery occlusion [162]. SPECT showed that cells accumulate in internal organs after administration in the femoral vein. 24 hours after carotid artery administration, most cells still accumulated in the peripheral organs, but some human neural progenitor cells were detected in the brain.
Since accumulation of nanoparticles in brain is often low, the signal-to-background ratio is usually poor. Therefore PET and SPECT imaging are hardly used for tracking nanoparticles in the brain. Yet, data have been presented on the imaging of liposomes carrying hemoglobin, as studied in a rat brain ischemia model caused by thrombosis of the middle cerebral artery [163]. For monitoring by μPET, the liposomes were labeled with 1-[^{18}F]fluoro-3,6-dioxatetracosane. The results indicated that liposome encapsulated hemoglobin can reduce the size of infarction, probably as a result of an improvement in the microcirculation and oxygen delivery. Similarly radiolabeled liposomes were also used to visualize brain tumors by means of PET. The leaky blood vessels in the tumor allowed passive accumulation of liposomes (size of approximately 100 nm) at the tumor site with a relatively low accumulation in the surrounding brain tissue [164]. The findings were confirmed by *ex vivo* autoradiography of brain slices. Accordingly, a similar approach may be useful for monitoring analogously liposomes or other well-defined nanocarriers for drug delivery to brain tumors.

8. Concluding remarks

Here we have summarized approaches for imaging nanoparticles and stem cells in(to) the brain. For (stem)cell-based delivery devices, imaging can provide information on location of the labeled cells, cell viability and the extent of therapeutic gene expression over prolonged periods of time. Imaging also allows *in vivo* tracking of nanocarriers over time, provided that the label does not interfere with the distribution of the nanocarrier. Imaging can also provide insight into the stability of nanocarriers and the release of their contents by comparing the distribution of the shell and the contents, labeled with distinct markers.

Over the past years, all major imaging modalities, including PET, SPECT, MRI and optical imaging have been applied for monitoring nanocarriers and delivery of associated/entrapped drugs into the brain Obviously, each modality has its own advantages and limitations, implying that the ideal carrier does not exist. The modality of choice strongly depends on the specific experimental and/or therapeutic aims. In addition, there is no ideal all-purpose labeling approach and consequently a labeling strategy should be selected that is most suitable for the specific delivery device involved. In general, however, the labeling agent should ideally be applicable in humans, nontoxic, safe to use, and easy to apply. In addition, the ideal labeling agent has a low background signal *in vivo*, is not released from the drug delivery device, is not affected by environmental factors, including biological fluids, and should not interfere with the crossing of the delivery vehicle across the BBB. Finally, the lifetime of the label should match the duration of experiment, but the signal of the label should disappear when the delivery device is degraded or stops functioning. Independent of which modality or labeling method is selected, adequate controls are essential, such as controls for the potential release of free tracer from the delivery device, and the localization of the delivery vehicle should be preferably confirmed by histological evidence.

When proper selection and validation of the tracer is performed, imaging of brain drug delivery devices can give an important contribution to research in the brain drug delivery field, including evidence-based optimization of the applied dose and dosing frequency, comparison of administration routes and prediction of therapeutic efficacy, long before the end of treatment. In addition, imaging can provide new insights into causes for failure of particular treatment strategies. Nanocarriers may not reach the brain in adequate quantities, whereas engineered cells may not produce the required therapeutic agent. In these cases it may be advantageous to consider an alternative administration route or drug carrier, rather than pursuing a new lead compound for drug development.

Current progress in *in vivo* molecular imaging includes multimodality imaging approaches. The aim of multimodality imaging is to overcome disadvantages of individual modalities, such as absence of anatomical details or low resolution. An interesting new development in this respect is the introduction of hybrid PET-MRI cameras, both for clinical and preclinical studies. These hybrid cameras not only combine the high sensitivity of PET with the excellent spatial resolution and soft tissue contrast of MRI, but would also allow tracking of dual labeled drug delivery devices. Although the impact of such hybrid imaging devices remains to be determined, it is clear that imaging techniques will remain playing an important role in the development and evaluation of devices that delivery drugs to the brain.

References

[1] Misra A, Ganesh S, Shahiwala A, Shah SP (2003) Drug delivery to the central nervous system: a review. J Pharm Pharm Sci 6: 252-273.
[2] Krauze MT, McKnight TR, Yamashita Y, Bringas J, Noble CO, Saito R, Geletneky K, Forsayeth J, Berger MS, Jackson P, Park JW, Bankiewicz KS (2005) Real-time visualization and characterization of liposomal delivery into the monkey brain by magnetic resonance imaging. Brain Res Brain Res Protoc 16: 20-26.
[3] Gogel S, Gubernator M, Minger SL (2011) Progress and prospects: stem cells and neurological diseases. Gene Ther 18: 1-6.
[4] Pardridge WM (2003) Blood-brain barrier drug targeting: the future of brain drug development. Mol Interv 3: 90-105, 151.
[5] Rubin LL, Staddon JM (1999) The cell biology of the blood-brain barrier. Annu Rev Neurosci 22: 11-28.
[6] Tiwari SB, Amiji MM (2006) A review of nanocarrier-based CNS delivery systems. Curr Drug Deliv 3: 219-232.
[7] Alvarez-Erviti L, Seow Y, Yin H, Betts C, Lakhal S, Wood MJA (2011) Delivery of siRNA to the mouse brain by systemic injection of targeted exosomes. Nat Biotech 29: 341-345.
[8] Moos T, Morgan EH (2001) Restricted transport of anti-transferrin receptor antibody (OX26) through the blood-brain barrier in the rat. J Neurochem 79: 119-129.
[9] Duffy KR, Pardridge WM (1987) Blood-brain barrier transcytosis of insulin in developing rabbits. Brain Res 420: 32-38.
[10] Kanwar JR, Sun X, Punj V, Sriramoju B, Mohan RR, Zhou SF, Chauhan A, Kanwar RK (2011) Nanoparticles in the treatment and diagnosis of neurological disorders: untamed dragon with fire power to heal. Nanomedicine.
[11] Tang Y, Shah K, Messerli SM, Snyder E, Breakefield X, Weissleder R (2003) In vivo tracking of neural progenitor cell migration to glioblastomas. Hum Gene Ther 14: 1247-1254.
[12] Bjugstad KB, Redmond DE, Jr., Teng YD, Elsworth JD, Roth RH, Blanchard BC, Snyder EY, Sladek JR, Jr. (2005) Neural stem cells implanted into MPTP-treated monkeys increase the size of endogenous tyrosine hydroxylase-positive cells found in the striatum: a return to control measures. Cell Transplant 14: 183-192.
[13] Kelly S, Bliss TM, Shah AK, Sun GH, Ma M, Foo WC, Masel J, Yenari MA, Weissman IL, Uchida N, Palmer T, Steinberg GK (2004) Transplanted human fetal neural stem cells survive, migrate, and differentiate in ischemic rat cerebral cortex. Proc Natl Acad Sci U S A 101: 11839-11844.
[14] Muller FJ, Snyder EY, Loring JF (2006) Gene therapy: can neural stem cells deliver? Nat Rev Neurosci 7: 75-84.
[15] Fischer UM, Harting MT, Jimenez F, Monzon-Posadas WO, Xue H, Savitz SI, Laine GA, Cox CS, Jr. (2009) Pulmonary passage is a major obstacle for intravenous stem cell delivery: the pulmonary first-pass effect. Stem Cells Dev 18: 683-692.
[16] Harting MT, Jimenez F, Xue H, Fischer UM, Baumgartner J, Dash PK, Cox CS (2009) Intravenous mesenchymal stem cell therapy for traumatic brain injury. J Neurosurg 110: 1189-1197.
[17] Stojanov K, de Vries EF, Hoekstra D, van Waarde A, Dierckx RA, Zuhorn IS (2011) [^{18}F]FDG labeling of neural stem cells for in vivo cell tracking with positron emission tomography: inhibition of tracer release by phloretin. Mol Imaging.
[18] Gao J, Dennis JE, Muzic RF, Lundberg M, Caplan AI (2001) The dynamic in vivo distribution of bone marrow-derived mesenchymal stem cells after infusion. Cells Tissues Organs 169: 12-20.
[19] Pirko I, Fricke ST, Johnson AJ, Rodriguez M, Macura SI (2005) Magnetic resonance imaging, microscopy, and spectroscopy of the central nervous system in experimental animals. NeuroRx 2: 250-264.

[20] Massoud TF, Gambhir SS (2003) Molecular imaging in living subjects: seeing fundamental biological processes in a new light. Genes Dev 17: 545-580.
[21] Choy G, Choyke P, Libutti SK (2003) Current advances in molecular imaging: noninvasive in vivo bioluminescent and fluorescent optical imaging in cancer research. Mol Imaging 2: 303-312.
[22] Weissleder R, Ntziachristos V (2003) Shedding light onto live molecular targets. Nat Med 9: 123-128.
[23] Rao J, Dragulescu-Andrasi A, Yao H (2007) Fluorescence imaging in vivo: recent advances. Curr Opin Biotechnol 18: 17-25.
[24] Zacharakis G, Kambara H, Shih H, Ripoll J, Grimm J, Saeki Y, Weissleder R, Ntziachristos V (2005) Volumetric tomography of fluorescent proteins through small animals in vivo. Proc Natl Acad Sci U S A 102: 18252-18257.
[25] Ntziachristos V, Ripoll J, Wang LV, Weissleder R (2005) Looking and listening to light: the evolution of whole-body photonic imaging. Nat Biotechnol 23: 313-320.
[26] Doyle TC, Burns SM, Contag CH (2004) In vivo bioluminescence imaging for integrated studies of infection. Cell Microbiol 6: 303-317.
[27] Chatziioannou AF (2005) Instrumentation for molecular imaging in preclinical research: Micro-PET and Micro-SPECT. Proc Am Thorac Soc 2: 533-536, 510-511.
[28] Rahmim A, Zaidi H (2008) PET versus SPECT: strengths, limitations and challenges. Nucl Med Commun 29: 193-207.
[29] Franc BL, Acton PD, Mari C, Hasegawa BH (2008) Small-animal SPECT and SPECT/CT: important tools for preclinical investigation. J Nucl Med 49: 1651-1663.
[30] Terreno E, Geninatti Crich S, Belfiore S, Biancone L, Cabella C, Esposito G, Manazza AD, Aime S (2006) Effect of the intracellular localization of a Gd-based imaging probe on the relaxation enhancement of water protons. Magn Reson Med 55: 491-497.
[31] Shen J, Cheng LN, Zhong XM, Duan XH, Guo RM, Hong GB (2010) Efficient in vitro labeling rabbit neural stem cell with paramagnetic Gd-DTPA and fluorescent substance. Eur J Radiol 75: 397-405.
[32] Cheng LN, Duan XH, Zhong XM, Guo RM, Zhang F, Zhou CP, Shen J (2011) Transplanted neural stem cells promote nerve regeneration in acute peripheral nerve traction injury: assessment using MRI. AJR Am J Roentgenol 196: 1381-1387.
[33] Modo M, Cash D, Mellodew K, Williams SC, Fraser SE, Meade TJ, Price J, Hodges H (2002) Tracking transplanted stem cell migration using bifunctional, contrast agent-enhanced, magnetic resonance imaging. Neuroimage 17: 803-811.
[34] Modo M, Mellodew K, Cash D, Fraser SE, Meade TJ, Price J, Williams SC (2004) Mapping transplanted stem cell migration after a stroke: a serial, in vivo magnetic resonance imaging study. Neuroimage 21: 311-317.
[35] Giesel FL, Stroick M, Griebe M, Troster H, von der Lieth CW, Requardt M, Rius M, Essig M, Kauczor HU, Hennerici MG, Fatar M (2006) Gadofluorine m uptake in stem cells as a new magnetic resonance imaging tracking method: an in vitro and in vivo study. Invest Radiol 41: 868-873.
[36] Montet-Abou K, Montet X, Weissleder R, Josephson L (2005) Transfection agent induced nanoparticle cell loading. Mol Imaging 4: 165-171.
[37] Kustermann E, Himmelreich U, Kandal K, Geelen T, Ketkar A, Wiedermann D, Strecker C, Esser J, Arnhold S, Hoehn M (2008) Efficient stem cell labeling for MRI studies. Contrast Media Mol Imaging 3: 27-37.
[38] Zhu J, Zhou L, XingWu F (2006) Tracking neural stem cells in patients with brain trauma. N Engl J Med 355: 2376-2378.
[39] Politi LS, Bacigaluppi M, Brambilla E, Cadioli M, Falini A, Comi G, Scotti G, Martino G, Pluchino S (2007) Magnetic-resonance-based tracking and quantification of intravenously injected neural stem cell accumulation in the brains of mice with experimental multiple sclerosis. Stem Cells 25: 2583-2592.

[40] Arbab AS, Yocum GT, Wilson LB, Parwana A, Jordan EK, Kalish H, Frank JA (2004) Comparison of transfection agents in forming complexes with ferumoxides, cell labeling efficiency, and cellular viability. Mol Imaging 3: 24-32.
[41] Modo M, Hoehn M, Bulte JW (2005) Cellular MR imaging. Mol Imaging 4: 143-164.
[42] Walczak P, Kedziorek DA, Gilad AA, Lin S, Bulte JW (2005) Instant MR labeling of stem cells using magnetoelectroporation. Magn Reson Med 54: 769-774.
[43] Shapiro EM, Skrtic S, Sharer K, Hill JM, Dunbar CE, Koretsky AP (2004) MRI detection of single particles for cellular imaging. Proc Natl Acad Sci U S A 101: 10901-10906.
[44] Hinds KA, Hill JM, Shapiro EM, Laukkanen MO, Silva AC, Combs CA, Varney TR, Balaban RS, Koretsky AP, Dunbar CE (2003) Highly efficient endosomal labeling of progenitor and stem cells with large magnetic particles allows magnetic resonance imaging of single cells. Blood 102: 867-872.
[45] Michalet X, Pinaud FF, Bentolila LA, Tsay JM, Doose S, Li JJ, Sundaresan G, Wu AM, Gambhir SS, Weiss S (2005) Quantum dots for live cells, in vivo imaging, and diagnostics. Science 307: 538-544.
[46] Lin S, Xie X, Patel MR, Yang YH, Li Z, Cao F, Gheysens O, Zhang Y, Gambhir SS, Rao JH, Wu JC (2007) Quantum dot imaging for embryonic stem cells. BMC Biotechnol 7: 67.
[47] So MK, Xu C, Loening AM, Gambhir SS, Rao J (2006) Self-illuminating quantum dot conjugates for in vivo imaging. Nat Biotechnol 24: 339-343.
[48] Pichler A, Prior JL, Piwnica-Worms D (2004) Imaging reversal of multidrug resistance in living mice with bioluminescence: MDR1 P-glycoprotein transports coelenterazine. Proc Natl Acad Sci U S A 101: 1702-1707.
[49] Elhami E, Goertzen AL, Xiang B, Deng J, Stillwell C, Mzengeza S, Arora RC, Freed D, Tian G (2011) Viability and proliferation potential of adipose-derived stem cells following labeling with a positron-emitting radiotracer. Eur J Nucl Med Mol Imaging 38: 1323-1334.
[50] Botti C, Negri DR, Seregni E, Ramakrishna V, Arienti F, Maffioli L, Lombardo C, Bogni A, Pascali C, Crippa F, Massaron S, Remonti F, Nerini-Molteni S, Canevari S, Bombardieri E (1997) Comparison of three different methods for radiolabelling human activated T lymphocytes. Eur J Nucl Med 24: 497-504.
[51] Adonai N, Nguyen KN, Walsh J, Iyer M, Toyokuni T, Phelps ME, McCarthy T, McCarthy DW, Gambhir SS (2002) Ex vivo cell labeling with 64Cu-pyruvaldehyde-bis(N4-methylthiosemicarbazone) for imaging cell trafficking in mice with positron-emission tomography. Proc Natl Acad Sci U S A 99: 3030-3035.
[52] Ma B, Hankenson KD, Dennis JE, Caplan AI, Goldstein SA, Kilbourn MR (2005) A simple method for stem cell labeling with fluorine 18. Nucl Med Biol 32: 701-705.
[53] Li ZB, Chen K, Wu Z, Wang H, Niu G, Chen X (2009) 64Cu-labeled PEGylated polyethylenimine for cell trafficking and tumor imaging. Mol Imaging Biol 11: 415-423.
[54] Chen K, Miao Z, Cheng Z (2011) In vivo PET imaging to track mesenchymal stem cells labelled with copper-64-pyruvaldehyde-bis (N4-methylthiosemicarbazone). J NUCL MED MEETING ABSTRACTS 52: 521-.
[55] de Labriolle-Vaylet C, Colas-Linhart N, Sala-Trepat M, Petiet A, Voisin P, Bok B (1998) Biological consequences of the heterogeneous irradiation of lymphocytes during technetium-99m hexamethylpropylene amine oxime white blood cell labelling. Eur J Nucl Med 25: 1423-1428.
[56] Fernandez P, Bordenave L, Celerier C, Bareille R, Brouillaud B, Basse-Cathalinat B (1999) A novel potential application for 99mTc-HMPAO: endothelial cell labeling for in vitro investigation of cell-biomaterial interactions. J Nucl Med 40: 1756-1763.
[57] Barbash IM, Chouraqui P, Baron J, Feinberg MS, Etzion S, Tessone A, Miller L, Guetta E, Zipori D, Kedes LH, Kloner RA, Leor J (2003) Systemic delivery of bone marrow-derived mesenchymal stem cells to the infarcted myocardium: feasibility, cell migration, and body distribution. Circulation 108: 863-868.

[58] Nowak B, Weber C, Schober A, Zeiffer U, Liehn EA, von Hundelshausen P, Reinartz P, Schaefer WM, Buell U (2007) Indium-111 oxine labelling affects the cellular integrity of haematopoietic progenitor cells. Eur J Nucl Med Mol Imaging 34: 715-721.
[59] Jin Y, Kong H, Stodilka RZ, Wells RG, Zabel P, Merrifield PA, Sykes J, Prato FS (2005) Determining the minimum number of detectable cardiac-transplanted 111In-tropolone-labelled bone-marrow-derived mesenchymal stem cells by SPECT. Phys Med Biol 50: 4445-4455.
[60] Bindslev L, Haack-Sorensen M, Bisgaard K, Kragh L, Mortensen S, Hesse B, Kjaer A, Kastrup J (2006) Labelling of human mesenchymal stem cells with indium-111 for SPECT imaging: effect on cell proliferation and differentiation. Eur J Nucl Med Mol Imaging 33: 1171-1177.
[61] Aicher A, Brenner W, Zuhayra M, Badorff C, Massoudi S, Assmus B, Eckey T, Henze E, Zeiher AM, Dimmeler S (2003) Assessment of the tissue distribution of transplanted human endothelial progenitor cells by radioactive labeling. Circulation 107: 2134-2139.
[62] Brenner W, Aicher A, Eckey T, Massoudi S, Zuhayra M, Koehl U, Heeschen C, Kampen WU, Zeiher AM, Dimmeler S, Henze E (2004) 111In-labeled CD34+ hematopoietic progenitor cells in a rat myocardial infarction model. J Nucl Med 45: 512-518.
[63] Kuyama J, McCormack A, George AJ, Heelan BT, Osman S, Batchelor JR, Peters AM (1997) Indium-111 labelled lymphocytes: isotope distribution and cell division. Eur J Nucl Med 24: 488-496.
[64] Eggert AA, Schreurs MW, Boerman OC, Oyen WJ, de Boer AJ, Punt CJ, Figdor CG, Adema GJ (1999) Biodistribution and vaccine efficiency of murine dendritic cells are dependent on the route of administration. Cancer Res 59: 3340-3345.
[65] Bestor TH (2000) Gene silencing as a threat to the success of gene therapy. J Clin Invest 105: 409-411.
[66] Gilad AA, Ziv K, McMahon MT, van Zijl PC, Neeman M, Bulte JW (2008) MRI reporter genes. J Nucl Med 49: 1905-1908.
[67] Cohen B, Dafni H, Meir G, Harmelin A, Neeman M (2005) Ferritin as an endogenous MRI reporter for noninvasive imaging of gene expression in C6 glioma tumors. Neoplasia 7: 109-117.
[68] Genove G, DeMarco U, Xu H, Goins WF, Ahrens ET (2005) A new transgene reporter for in vivo magnetic resonance imaging. Nat Med 11: 450-454.
[69] Nakamura C, Burgess JG, Sode K, Matsunaga T (1995) An iron-regulated gene, magA, encoding an iron transport protein of Magnetospirillum sp. strain AMB-1. J Biol Chem 270: 28392-28396.
[70] Nakamura C, Kikuchi T, Burgess JG, Matsunaga T (1995) Iron-regulated expression and membrane localization of the magA protein in Magnetospirillum sp. strain AMB-1. J Biochem 118: 23-27.
[71] Zurkiya O, Chan AW, Hu X (2008) MagA is sufficient for producing magnetic nanoparticles in mammalian cells, making it an MRI reporter. Magn Reson Med 59: 1225-1231.
[72] Faivre D, Schuler D (2008) Magnetotactic bacteria and magnetosomes. Chem Rev 108: 4875-4898.
[73] Deliolanis NC, Kasmieh R, Wurdinger T, Tannous BA, Shah K, Ntziachristos V (2008) Performance of the red-shifted fluorescent proteins in deep-tissue molecular imaging applications. J Biomed Opt 13: 044008.
[74] Patterson GH, Knobel SM, Sharif WD, Kain SR, Piston DW (1997) Use of the green fluorescent protein and its mutants in quantitative fluorescence microscopy. Biophys J 73: 2782-2790.
[75] Shaner NC, Campbell RE, Steinbach PA, Giepmans BN, Palmer AE, Tsien RY (2004) Improved monomeric red, orange and yellow fluorescent proteins derived from Discosoma sp. red fluorescent protein. Nat Biotechnol 22: 1567-1572.
[76] Wang L, Jackson WC, Steinbach PA, Tsien RY (2004) Evolution of new nonantibody proteins via iterative somatic hypermutation. Proc Natl Acad Sci U S A 101: 16745-16749.
[77] Shcherbo D, Merzlyak EM, Chepurnykh TV, Fradkov AF, Ermakova GV, Solovieva EA, Lukyanov KA, Bogdanova EA, Zaraisky AG, Lukyanov S, Chudakov DM (2007) Bright far-red fluorescent protein for whole-body imaging. Nat Methods 4: 741-746.

[78] Billinton N, Knight AW (2001) Seeing the wood through the trees: a review of techniques for distinguishing green fluorescent protein from endogenous autofluorescence. Anal Biochem 291: 175-197.
[79] Boulnois J-L (1986) Photophysical processes in recent medical laser developments: A review. Lasers in Medical Science 1: 47-66.
[80] Fraga H (2008) Firefly luminescence: a historical perspective and recent developments. Photochem Photobiol Sci 7: 146-158.
[81] Roda A, Guardigli M, Michelini E, Mirasoli M (2009) Nanobioanalytical luminescence: Forster-type energy transfer methods. Anal Bioanal Chem 393: 109-123.
[82] Wood KV, Lam YA, Seliger HH, McElroy WD (1989) Complementary DNA coding click beetle luciferases can elicit bioluminescence of different colors. Science 244: 700-702.
[83] Lorenz WW, McCann RO, Longiaru M, Cormier MJ (1991) Isolation and expression of a cDNA encoding Renilla reniformis luciferase. Proc Natl Acad Sci U S A 88: 4438-4442.
[84] Loening AM, Wu AM, Gambhir SS (2007) Red-shifted Renilla reniformis luciferase variants for imaging in living subjects. Nat Methods 4: 641-643.
[85] Ji X, Cheng L, Wei F, Li H, Wang M, Tian Y, Chen X, Wang Y, Wolf F, Li C, Huang Q (2009) Noninvasive visualization of retinoblastoma growth and metastasis via bioluminescence imaging. Invest Ophthalmol Vis Sci 50: 5544-5551.
[86] Tannous BA, Kim DE, Fernandez JL, Weissleder R, Breakefield XO (2005) Codon-optimized Gaussia luciferase cDNA for mammalian gene expression in culture and in vivo. Mol Ther 11: 435-443.
[87] Close DM, Patterson SS, Ripp S, Baek SJ, Sanseverino J, Sayler GS (2010) Autonomous bioluminescent expression of the bacterial luciferase gene cassette (lux) in a mammalian cell line. PLoS One 5: e12441.
[88] de Almeida PE, van Rappard JR, Wu JC (2011) In vivo bioluminescence for tracking cell fate and function. Am J Physiol Heart Circ Physiol 301: H663-671.
[89] Zhang Y, Bressler JP, Neal J, Lal B, Bhang HE, Laterra J, Pomper MG (2007) ABCG2/BCRP expression modulates D-Luciferin based bioluminescence imaging. Cancer Res 67: 9389-9397.
[90] Meighen EA (1991) Molecular biology of bacterial bioluminescence. Microbiol Rev 55: 123-142.
[91] Acton PD, Zhou R (2005) Imaging reporter genes for cell tracking with PET and SPECT. Q J Nucl Med Mol Imaging 49: 349-360.
[92] Tjuvajev JG, Doubrovin M, Akhurst T, Cai S, Balatoni J, Alauddin MM, Finn R, Bornmann W, Thaler H, Conti PS, Blasberg RG (2002) Comparison of radiolabeled nucleoside probes (FIAU, FHBG, and FHPG) for PET imaging of HSV1-tk gene expression. J Nucl Med 43: 1072-1083.
[93] MacLaren DC, Gambhir SS, Satyamurthy N, Barrio JR, Sharfstein S, Toyokuni T, Wu L, Berk AJ, Cherry SR, Phelps ME, Herschman HR (1999) Repetitive, non-invasive imaging of the dopamine D2 receptor as a reporter gene in living animals. Gene Ther 6: 785-791.
[94] Auricchio A, Acton PD, Hildinger M, Louboutin JP, Plossl K, O'Connor E, Kung HF, Wilson JM (2003) In vivo quantitative noninvasive imaging of gene transfer by single-photon emission computerized tomography. Hum Gene Ther 14: 255-261.
[95] Shin JH, Chung JK, Kang JH, Lee YJ, Kim KI, So Y, Jeong JM, Lee DS, Lee MC (2004) Noninvasive imaging for monitoring of viable cancer cells using a dual-imaging reporter gene. J Nucl Med 45: 2109-2115.
[96] Zinn KR, Buchsbaum DJ, Chaudhuri TR, Mountz JM, Grizzle WE, Rogers BE (2000) Noninvasive monitoring of gene transfer using a reporter receptor imaged with a high-affinity peptide radiolabeled with 99mTc or 188Re. J Nucl Med 41: 887-895.
[97] Rogers BE, Chaudhuri TR, Reynolds PN, Della Manna D, Zinn KR (2003) Non-invasive gamma camera imaging of gene transfer using an adenoviral vector encoding an epitope-tagged receptor as a reporter. Gene Ther 10: 105-114.

[98] Doubrovin M, Ponomarev V, Serganova I, Soghomonian S, Myagawa T, Beresten T, Ageyeva L, Sadelain M, Koutcher J, Blasberg RG, Tjuvajev JG (2003) Development of a new reporter gene system--dsRed/xanthine phosphoribosyltransferase-xanthine for molecular imaging of processes behind the intact blood-brain barrier. Mol Imaging 2: 93-112.
[99] Vandeputte C, Evens N, Toelen J, Deroose CM, Bosier B, Ibrahimi A, Van der Perren A, Gijsbers R, Janssen P, Lambert DM, Verbruggen A, Debyser Z, Bormans G, Baekelandt V, Van Laere K (2011) A PET brain reporter gene system based on type 2 cannabinoid receptors. J Nucl Med 52: 1102-1109.
[100] Maresz K, Carrier EJ, Ponomarev ED, Hillard CJ, Dittel BN (2005) Modulation of the cannabinoid CB2 receptor in microglial cells in response to inflammatory stimuli. J Neurochem 95: 437-445.
[101] Unger EC, MacDougall P, Cullis P, Tilcock C (1989) Liposomal Gd-DTPA: effect of encapsulation on enhancement of hepatoma model by MRI. Magn Reson Imaging 7: 417-423.
[102] Saito R, Bringas JR, McKnight TR, Wendland MF, Mamot C, Drummond DC, Kirpotin DB, Park JW, Berger MS, Bankiewicz KS (2004) Distribution of liposomes into brain and rat brain tumor models by convection-enhanced delivery monitored with magnetic resonance imaging. Cancer Res 64: 2572-2579.
[103] Saito R, Krauze MT, Bringas JR, Noble C, McKnight TR, Jackson P, Wendland MF, Mamot C, Drummond DC, Kirpotin DB, Hong K, Berger MS, Park JW, Bankiewicz KS (2005) Gadolinium-loaded liposomes allow for real-time magnetic resonance imaging of convection-enhanced delivery in the primate brain. Exp Neurol 196: 381-389.
[104] Kabalka G, Buonocore E, Hubner K, Moss T, Norley N, Huang L (1987) Gadolinium-labeled liposomes: targeted MR contrast agents for the liver and spleen. Radiology 163: 255-258.
[105] Kozlowska D, Foran P, MacMahon P, Shelly MJ, Eustace S, O'Kennedy R (2009) Molecular and magnetic resonance imaging: The value of immunoliposomes. Adv Drug Deliv Rev 61: 1402-1411.
[106] Elmi MM, Sarbolouki MN (2001) A simple method for preparation of immuno-magnetic liposomes. Int J Pharm 215: 45-50.
[107] Martina MS, Fortin JP, Menager C, Clement O, Barratt G, Grabielle-Madelmont C, Gazeau F, Cabuil V, Lesieur S (2005) Generation of superparamagnetic liposomes revealed as highly efficient MRI contrast agents for in vivo imaging. J Am Chem Soc 127: 10676-10685.
[108] Hickey RJ, Haynes AS, Kikkawa JM, Park SJ (2011) Controlling the self-assembly structure of magnetic nanoparticles and amphiphilic block-copolymers: from micelles to vesicles. J Am Chem Soc 133: 1517-1525.
[109] Sanson C, Diou O, Thevenot J, Ibarboure E, Soum A, Brulet A, Miraux S, Thiaudiere E, Tan S, Brisson A, Dupuis V, Sandre O, Lecommandoux S (2011) Doxorubicin loaded magnetic polymersomes: theranostic nanocarriers for MR imaging and magneto-chemotherapy. ACS Nano 5: 1122-1140.
[110] Lu W, Zhang Y, Tan YZ, Hu KL, Jiang XG, Fu SK (2005) Cationic albumin-conjugated pegylated nanoparticles as novel drug carrier for brain delivery. J Control Release 107: 428-448.
[111] Pang Z, Lu W, Gao H, Hu K, Chen J, Zhang C, Gao X, Jiang X, Zhu C (2008) Preparation and brain delivery property of biodegradable polymersomes conjugated with OX26. J Control Release 128: 120-127.
[112] Hadaczek P, Yamashita Y, Mirek H, Tamas L, Bohn MC, Noble C, Park JW, Bankiewicz K (2006) The "perivascular pump" driven by arterial pulsation is a powerful mechanism for the distribution of therapeutic molecules within the brain. Mol Ther 14: 69-78.
[113] Deissler V, Ruger R, Frank W, Fahr A, Kaiser WA, Hilger I (2008) Fluorescent liposomes as contrast agents for in vivo optical imaging of edemas in mice. Small 4: 1240-1246.

[114] He X, Na MH, Kim JS, Lee GY, Park JY, Hoffman AS, Nam JO, Han SE, Sim GY, Oh YK, Kim lS, Lee BH (2011) A novel peptide probe for imaging and targeted delivery of liposomal doxorubicin to lung tumor. Mol Pharm 8: 430-438.
[115] Nobs L, Buchegger F, Gurny R, Allemann E (2004) Current methods for attaching targeting ligands to liposomes and nanoparticles. J Pharm Sci 93: 1980-1992.
[116] Harrington KJ, Rowlinson-Busza G, Syrigos KN, Uster PS, Vile RG, Stewart JS (2000) Pegylated liposomes have potential as vehicles for intratumoral and subcutaneous drug delivery. Clin Cancer Res 6: 2528-2537.
[117] Levchenko TS, Rammohan R, Lukyanov AN, Whiteman KR, Torchilin VP (2002) Liposome clearance in mice: the effect of a separate and combined presence of surface charge and polymer coating. Int J Pharm 240: 95-102.
[118] Phillips WT, Goins BA, Bao A (2009) Radioactive liposomes. Wiley Interdiscip Rev Nanomed Nanobiotechnol 1: 69-83.
[119] Andreozzi E, Seo JW, Ferrara K, Louie A (2011) Novel method to label solid lipid nanoparticles with 64cu for positron emission tomography imaging. Bioconjug Chem 22: 808-818.
[120] Harivardhan Reddy L, Sharma RK, Chuttani K, Mishra AK, Murthy RS (2005) Influence of administration route on tumor uptake and biodistribution of etoposide loaded solid lipid nanoparticles in Dalton's lymphoma tumor bearing mice. J Control Release 105: 185-198.
[121] Upadhyay KK, Bhatt AN, Castro E, Mishra AK, Chuttani K, Dwarakanath BS, Schatz C, Le Meins JF, Misra A, Lecommandoux S (2010) In vitro and in vivo evaluation of docetaxel loaded biodegradable polymersomes. Macromol Biosci 10: 503-512.
[122] Chertok B, Cole AJ, David AE, Yang VC (2010) Comparison of electron spin resonance spectroscopy and inductively-coupled plasma optical emission spectroscopy for biodistribution analysis of iron-oxide nanoparticles. Mol Pharm 7: 375-385.
[123] Wenger Y, Schneider RJ, 2nd, Reddy GR, Kopelman R, Jolliet O, Philbert MA (2011) Tissue distribution and pharmacokinetics of stable polyacrylamide nanoparticles following intravenous injection in the rat. Toxicol Appl Pharmacol 251: 181-190.
[124] Calvo P, Gouritin B, Chacun H, Desmaele D, D'Angelo J, Noel JP, Georgin D, Fattal E, Andreux JP, Couvreur P (2001) Long-circulating PEGylated polycyanoacrylate nanoparticles as new drug carrier for brain delivery. Pharm Res 18: 1157-1166.
[125] Vinogradov SV, Batrakova EV, Kabanov AV (2004) Nanogels for oligonucleotide delivery to the brain. Bioconjug Chem 15: 50-60.
[126] Costantino L, Gandolfi F, Tosi G, Rivasi F, Vandelli MA, Forni F (2005) Peptide-derivatized biodegradable nanoparticles able to cross the blood-brain barrier. J Control Release 108: 84-96.
[127] Weiss CK, Kohnle MV, Landfester K, Hauk T, Fischer D, Schmitz-Wienke J, Mailander V (2008) The first step into the brain: uptake of NIO-PBCA nanoparticles by endothelial cells in vitro and in vivo, and direct evidence for their blood-brain barrier permeation. ChemMedChem 3: 1395-1403.
[128] Zensi A, Begley D, Pontikis C, Legros C, Mihoreanu L, Wagner S, Buchel C, von Briesen H, Kreuter J (2009) Albumin nanoparticles targeted with Apo E enter the CNS by transcytosis and are delivered to neurones. J Control Release 137: 78-86.
[129] Khor SP, Mayersohn M (1991) Potential error in the measurement of tissue to blood distribution coefficients in physiological pharmacokinetic modeling. Residual tissue blood. I. Theoretical considerations. Drug Metab Dispos 19: 478-485.
[130] Khor SP, Bozigian H, Mayersohn M (1991) Potential error in the measurement of tissue to blood distribution coefficients in physiological pharmacokinetic modeling. Residual tissue blood. II. Distribution of phencyclidine in the rat. Drug Metab Dispos 19: 486-490.
[131] Lee YJ, Kusuhara H, Jonker JW, Schinkel AH, Sugiyama Y (2005) Investigation of efflux transport of dehydroepiandrosterone sulfate and mitoxantrone at the mouse blood-brain barrier: a minor role of breast cancer resistance protein. J Pharmacol Exp Ther 312: 44-52.

[132] Triguero D, Buciak J, Pardridge WM (1990) Capillary depletion method for quantification of blood-brain barrier transport of circulating peptides and plasma proteins. J Neurochem 54: 1882-1888.
[133] Gutierrez EG, Banks WA, Kastin AJ (1993) Murine tumor necrosis factor alpha is transported from blood to brain in the mouse. J Neuroimmunol 47: 169-176.
[134] Gosk S, Vermehren C, Storm G, Moos T (2004) Targeting anti-transferrin receptor antibody (OX26) and OX26-conjugated liposomes to brain capillary endothelial cells using in situ perfusion. J Cereb Blood Flow Metab 24: 1193-1204.
[135] Sakamoto A, Ido T (1993) Liposome targeting to rat brain: effect of osmotic opening of the blood-brain barrier. Brain Res 629: 171-175.
[136] Sugiyama T, Kuroda S, Osanai T, Shichinohe H, Kuge Y, Ito M, Kawabori M, Iwasaki Y (2011) Near-infrared fluorescence labeling allows noninvasive tracking of bone marrow stromal cells transplanted into rat infarct brain. Neurosurgery 68: 1036-1047; discussion 1047.
[137] Miletic H, Fischer Y, Litwak S, Giroglou T, Waerzeggers Y, Winkeler A, Li H, Himmelreich U, Lange C, Stenzel W, Deckert M, Neumann H, Jacobs AH, von Laer D (2007) Bystander killing of malignant glioma by bone marrow-derived tumor-infiltrating progenitor cells expressing a suicide gene. Mol Ther 15: 1373-1381.
[138] Zhao D, Najbauer J, Garcia E, Metz MZ, Gutova M, Glackin CA, Kim SU, Aboody KS (2008) Neural stem cell tropism to glioma: critical role of tumor hypoxia. Mol Cancer Res 6: 1819-1829.
[139] Rao KS, Reddy MK, Horning JL, Labhasetwar V (2008) TAT-conjugated nanoparticles for the CNS delivery of anti-HIV drugs. Biomaterials 29: 4429-4438.
[140] Sousa F, Mandal S, Garrovo C, Astolfo A, Bonifacio A, Latawiec D, Menk RH, Arfelli F, Huewel S, Legname G, Galla HJ, Krol S (2010) Functionalized gold nanoparticles: a detailed in vivo multimodal microscopic brain distribution study. Nanoscale 2: 2826-2834.
[141] Deroose CM, Reumers V, Gijsbers R, Bormans G, Debyser Z, Mortelmans L, Baekelandt V (2006) Noninvasive monitoring of long-term lentiviral vector-mediated gene expression in rodent brain with bioluminescence imaging. Mol Ther 14: 423-431.
[142] Callera F, de Melo CM (2007) Magnetic resonance tracking of magnetically labeled autologous bone marrow CD34+ cells transplanted into the spinal cord via lumbar puncture technique in patients with chronic spinal cord injury: CD34+ cells' migration into the injured site. Stem Cells Dev 16: 461-466.
[143] Walczak P, Kedziorek DA, Gilad AA, Barnett BP, Bulte JW (2007) Applicability and limitations of MR tracking of neural stem cells with asymmetric cell division and rapid turnover: the case of the shiverer dysmyelinated mouse brain. Magn Reson Med 58: 261-269.
[144] Alexiou C, Arnold W, Klein RJ, Parak FG, Hulin P, Bergemann C, Erhardt W, Wagenpfeil S, Lubbe AS (2000) Locoregional cancer treatment with magnetic drug targeting. Cancer Res 60: 6641-6648.
[145] Lubbe AS, Alexiou C, Bergemann C (2001) Clinical applications of magnetic drug targeting. J Surg Res 95: 200-206.
[146] Chertok B, David AE, Huang Y, Yang VC (2007) Glioma selectivity of magnetically targeted nanoparticles: a role of abnormal tumor hydrodynamics. J Control Release 122: 315-323.
[147] Cole AJ, David AE, Wang J, Galban CJ, Hill HL, Yang VC (2011) Polyethylene glycol modified, cross-linked starch-coated iron oxide nanoparticles for enhanced magnetic tumor targeting. Biomaterials 32: 2183-2193.
[148] Cole AJ, David AE, Wang J, Galban CJ, Yang VC (2011) Magnetic brain tumor targeting and biodistribution of long-circulating PEG-modified, cross-linked starch-coated iron oxide nanoparticles. Biomaterials 32: 6291-6301.
[149] Raghavan R, Brady ML, Rodriguez-Ponce MI, Hartlep A, Pedain C, Sampson JH (2006) Convection-enhanced delivery of therapeutics for brain disease, and its optimization. Neurosurg Focus 20: E12.

[150] Shah K, Bureau E, Kim DE, Yang K, Tang Y, Weissleder R, Breakefield XO (2005) Glioma therapy and real-time imaging of neural precursor cell migration and tumor regression. Ann Neurol 57: 34-41.
[151] Ntziachristos V (2006) Fluorescence molecular imaging. Annu Rev Biomed Eng 8: 1-33.
[152] McCann CM, Waterman P, Figueiredo JL, Aikawa E, Weissleder R, Chen JW (2009) Combined magnetic resonance and fluorescence imaging of the living mouse brain reveals glioma response to chemotherapy. Neuroimage 45: 360-369.
[153] Hyde D, de Kleine R, MacLaurin SA, Miller E, Brooks DH, Krucker T, Ntziachristos V (2009) Hybrid FMT-CT imaging of amyloid-beta plaques in a murine Alzheimer's disease model. Neuroimage 44: 1304-1311.
[154] Levasseur JE, Wei EP, Raper AJ, Kontos AA, Patterson JL (1975) Detailed description of a cranial window technique for acute and chronic experiments. Stroke 6: 308-317.
[155] Grutzendler J, Kasthuri N, Gan WB (2002) Long-term dendritic spine stability in the adult cortex. Nature 420: 812-816.
[156] Drew PJ, Shih AY, Driscoll JD, Knutsen PM, Blinder P, Davalos D, Akassoglou K, Tsai PS, Kleinfeld D (2010) Chronic optical access through a polished and reinforced thinned skull. Nat Methods 7: 981-984.
[157] Campbell RB, Fukumura D, Brown EB, Mazzola LM, Izumi Y, Jain RK, Torchilin VP, Munn LL (2002) Cationic charge determines the distribution of liposomes between the vascular and extravascular compartments of tumors. Cancer Res 62: 6831-6836.
[158] Dreher MR, Liu W, Michelich CR, Dewhirst MW, Yuan F, Chilkoti A (2006) Tumor vascular permeability, accumulation, and penetration of macromolecular drug carriers. J Natl Cancer Inst 98: 335-344.
[159] Nakamura T, Dhawan V, Chaly T, Fukuda M, Ma Y, Breeze R, Greene P, Fahn S, Freed C, Eidelberg D (2001) Blinded positron emission tomography study of dopamine cell implantation for Parkinson's disease. Ann Neurol 50: 181-187.
[160] Wang J, Tian M, Zhang H (2011) PET molecular imaging in stem cell therapy for neurological diseases. Eur J Nucl Med Mol Imaging 38: 1926-1938.
[161] Moolten FL, Wells JM (1990) Curability of tumors bearing herpes thymidine kinase genes transferred by retroviral vectors. J Natl Cancer Inst 82: 297-300.
[162] Lappalainen RS, Narkilahti S, Huhtala T, Liimatainen T, Suuronen T, Narvanen A, Suuronen R, Hovatta O, Jolkkonen J (2008) The SPECT imaging shows the accumulation of neural progenitor cells into internal organs after systemic administration in middle cerebral artery occlusion rats. Neurosci Lett 440: 246-250.
[163] Urakami T, Kawaguchi AT, Akai S, Hatanaka K, Koide H, Shimizu K, Asai T, Fukumoto D, Harada N, Tsukada H, Oku N (2009) In vivo distribution of liposome-encapsulated hemoglobin determined by positron emission tomography. Artif Organs 33: 164-168.
[164] Oku N, Yamashita M, Katayama Y, Urakami T, Hatanaka K, Shimizu K, Asai T, Tsukada H, Akai S, Kanazawa H (2011) PET imaging of brain cancer with positron emitter-labeled liposomes. Int J Pharm 403: 170-177.